KTH Engineering Sciences

Tandem optical parametric oscillators using volume Bragg grating spectral control

Markus Henriksson

Doctoral Thesis

Department of Applied Physics
Royal Institute of Technology
Stockholm, Sweden 2010

Tandem optical parametric oscillators using volume Bragg grating spectral control

Laser Physics
Department of Applied Physics
Royal Institute of Technology
Roslagstullsbacken 21
SE-106 91 Stockholm, Sweden

Akademisk avhandling som med tillstånd av Kungliga Tekniska Högskolan framlägges till offentlig granskning för avläggande av teknologie doktorsexamen fredagen den 4 juni 2010, kl. 13.00, sal FA32, Albanova, Roslagstullsbacken 21, Stockholm. Avhandlingen kommer att försvaras på engelska.

TRITA-FYS 2010:21
ISSN 0280-316X
ISRN KTH/FYS/--10:21--SE
ISBN 978-91-7415-626-3

Cover picture: Optical parametric oscillator seen through the input coupling mirror. The green light emitted from the PPKTP crystal is parasitic second harmonic generation.

Printed by Universitetsservice US AB, Stockholm 2010

Markus Henriksson
Tandem optical parametric oscillators using volume Bragg grating spectral control
Laser Physics, Department of Applied Physics, KTH - Royal Institute of Technology, 106 91 Stockholm, Sweden
ISBN 978-91-7415-626-3, TRITA-FYS 2010:21, ISSN 0280-316X, ISRN KTH/FYS/--10:21--SE

Abstract

This thesis describes research on near degenerate quasi phase-matched optical parametric oscillators (OPO) where volume Bragg gratings (VBG) are used to produce narrow oscillation bandwidth. These OPOs are then used to pump a second OPO to generate mid-infrared radiation.

The atmospheric transmission windows in the 3.5 to 5 μm wavelength region are used for seekers on infrared homing missiles. These missiles are available to guerrilla and terrorist groups and have been used in a number of attacks on military and civilian aircraft. Laser sources at the same wavelengths are an important component in countermeasure systems for aircraft self-protection. Similar laser sources also have applications in laser surgery.

At wavelengths longer than 4 μm crystal materials for multi-Watt level average power nonlinear devices is a problem. The best solution so far is to use $ZnGeP_2$ (ZGP). ZGP and the available alternatives all have a problem of near-infrared absorption, and a mid-infrared OPO thus has to use a pump wavelength near 2 μm. This pump source can be a neodymium laser at 1.06 μm with a near degenerate OPO. Nonlinear devices for low to medium pulse energies are dominated by quasi phase-matched materials because of their higher effective nonlinearities and lack of walk-off. In addition they allow type I interaction where signal and idler from the OPO have the same polarization, which has the advantage that both waves can be used to pump the ZGP OPO. The drawback of this is that the near-degenerate interaction has very wide gain bandwidth. Efficient pumping of the second OPO demands narrow bandwidth output from the first OPO.

Volume Bragg gratings that are glass materials with a periodic refractive index modulation have emerged as high quality narrow bandwidth reflectors. By using a VBG as one cavity mirror in an OPO the feedback bandwidth and hence the OPO oscillation bandwidth can be kept very narrow. Signal and idler bandwidths of 10 and 20 GHz (FWHM) at 2122 and 2135 nm, respectively, have been demonstrated. This should be compared to the several hundred nanometre bandwidth from an OPO using dielectric mirrors. Very narrow bandwidth operation has been achieved so close to degeneracy that the signal and idler are not resolvable.

The total output energy generated in the PPKTP OPO (signal and idler together) has been used to pump a ZGP OPO that produced mid-IR radiation. Tuning of the signal from a ZGP OPO from 2.9 μm to degeneracy at 4.3 μm has been shown, with a corresponding idler wavelength tuneable up to 8 μm. The highest conversion efficiency that has been reached from 1.06 μm to the mid-IR was 12 %. This setup used a PPKTP OPO with 30 % conversion efficiency and 13 nm separation of signal and idler (2122 and 2135 nm). The pulse repetition frequency was 20 kHz and the generated output power in the mid-IR was 3.2 W.

Keywords: optical parametric oscillators, mid-infrared, volume Bragg gratings, PPKTP, ZGP, nonlinear optics, narrowband OPO

Sammanfattning

Den här avhandlingen beskriver forskning om kvasifasmatchade optiska parametriska oscillatorer (OPO) nära degeneration där volymbraggitter (VBG) används för att begränsa den spektrala bandbredden. Dessa OPOer används sedan för att pumpa en andra OPO för att generera laserstrålning i mellanvågs-IR.

Atmosfärens transmissionsfönster i våglängdsbandet 3,5 till 5 μm används för målsökare i värmesökande robotar. Denna typ av robotar finns hos gerilla- och terroristgrupper och har använts för attacker mot både militära och civila mål. Laserkällor i samma våglängdsområde är en viktig komponent i motmedelssystem för egenskydd av flygplan och helikoptrar. Liknande laserkällor har även tillämpningar inom laserkirurgi.

Kristallmaterial för ickelinjär optik med medeleffekter på flera Watt vid våglängder över 4 μm är ett problem. Den bästa tillgängliga lösningen är att använda $ZnGeP_2$ (ZGP). ZGP och de alternativ som finns begränsas alla av absorption i det nära infraröda området och OPOer för generering av mellanvågs-IR måste därför använda en pumpvåglängd runt 2 μm. Pumpkällan kan antingen vara en holmiumlaser eller en neodymlaser vid 1,06 μm med en OPO nära degeneration. Eftersom neodymlasrar är kommersiellt tillgängliga är den andra lösningen i de flesta fall att föredra. I OPOer med låga eller måttliga pumpenergier används vanligtvis kvasifasmatchade material på grund av att de ger tillgång till starkare effektiv ickelinjaritet och undviker walk-off. Dessutom tillåter de typ I fasmatchning där signal och idler från OPOn har samma polarisation, vilket har fördelen att båda kan användas för att pumpa ZGP OPOn. Nackdelen är att förstärkningsbandbredden blir väldigt stor nära degeneration. Effektiv pumpning av den andra OPOn kräver samtidigt smalbandig strålning från den första OPOn.

Volymbraggitter är glasmaterial med periodisk modulation av brytningsindex och har utvecklats till smalbandiga reflektorer med hög kvalitet. Genom att använda ett VBG som kavitetsspegel i en OPO begränsas bandbredden på den återkopplade strålningen och OPOn kan hållas smalbandig. Bandbredder på signal och idler på 10 och 20 GHz vid 2122 och 2135 nm, respektive, har visats. Detta ska jämföras med de flera hundra nanometer som fås från motsvarande OPO med dielektriska speglar. OPOn kan även arbeta så nära degeneration att signal och idler inte är separerade, fortfarande med smal bandbredd.

All den genererade strålningen från PPKTP OPOn (signal och idler tillsammans) har använts som pump för en ZGP OPO som genererade strålning i mellanvågs-IR. Signalen från ZGP OPO kunde stämmas av från 2,9 μm till degeneration vid 4,3 μm, med en tillhörande idler som stämmer ut till 8 μm. Den högsta uppnådda konverteringsgraden från 1,06 μm till mellanvågs-IR var 12 %. Den uppställningen använde en PPKTP OPO med 30 % konverteringsgrad och 13 nm separation mellan signal och idler (2122 och 2135 nm). Pulsrepetitionsfrekvensen var 20 kHz och den totala uteffekten i 3,5 till 5 μm området var 3,2 W.

Contents

List of publications

Publications included in the thesis

I. M. Henriksson, L. Sjöqvist, V. Pasiskevicius and F. Laurell, *Narrow linewidth 2 μm optical parametric oscillation in periodically poled $LiNbO_3$ with volume Bragg grating outcoupler,* Applied Physics B: Lasers and Optics **86**, 497-501 (2007).

II. M. Henriksson, M. Tiihonen, V. Pasiskevicius and F. Laurell, *$ZnGeP_2$ parametric oscillator pumped by a linewidth-narrowed parametric 2 μm source*, Optics Letters **31**, 1878-1880 (2006).

III. M. Henriksson, M. Tiihonen, V. Pasiskevicius and F. Laurell, *Mid-infrared ZGP OPO pumped by near-degenerate narrowband type-I PPKTP parametric oscillator*, Applied Physics B: Lasers and Optics **88**, 37-41 (2007).

IV. M. Henriksson, L. Sjöqvist, V. Pasiskevicius and F. Laurell, *Spectrum of Multi-Longitudinal Mode Pumped Near-Degenerate OPOs with Volume Bragg Grating Output Couplers*, Optics Express **17**, 17582-17589 (2009).

V. M. Henriksson, L. Sjöqvist, V. Pasiskevicius and F. Laurell, *Cavity length resonances in a nanosecond singly resonant optical parametric oscillator*, submitted to Optics Express april 2010.

Publications not included in the thesis

Papers in international refereed journals

A1. M. Henriksson, *Detection probabilities for photon-counting avalanche photodiodes applied to a laser radar system,* Applied Optics **44**, 5140-5147 (2005).

A2. A. Saddington, M. Richardson, S. Ritchie, K. Knowles, D. Titterton, L. Sjöqvist and M. Henriksson, *The Aero-Optical Effects of a DIRCM Pod in the Transonic Regime,* submitted to AIAA Journal, January 2010.

Other thesis

A3. M. Henriksson, *Nanosecond tandem optical parametric oscillators for mid-infrared generation,* Licentiate thesis, KTH - Royal Institute of Technology, Stockholm, Sweden, TRITA-FYS 2006:83, ISBN 978-91-7178-552-7 (2006).

Patents

A4. M. Henriksson, V. Pasiskevicius and F. Laurell, *Laserkälla för det infraröda våglängdsområdet*, Swedish patent nr 0502396-5 (2007).

Conference proceedings and presentations

A5. P. Jonsson, H. Habberstad, M. Henriksson, D. Letalick and T. Carlsson, *Detection of buried land mines using acoustic excitation and a fiber-based coherent laser radar,* Coherent laser radar conference (Bar Harbor, USA, 2003).

A6. D. Letalick, T. Carlsson, H. Habberstad and M. Henriksson, *Target recognition by vibration frequency analysis - a comparison of laser vibrometry and acoustic methods,* Proc. SPIE 5086, 246-252 (2003).

A7. O. Steinvall, L. Klasen, C. Grönwall, U. Soderman, S. Ahlberg, Å. Persson, M. Elmqvist, H. Larsson, D. Letalick, P. Andersson, T. Carlsson and M. Henriksson, *3D laser sensing at FOI: overview and a system perspective,* Proc. SPIE 5412, 294-309 (2004).

A8. L. Sjöqvist, O. Gustafsson and M. Henriksson, *Laser beam propagation in close vicinity to a downscaled jet engine exhaust,* Proc. SPIE 5615, 137-148 (2004).

A9. M. Henriksson, L. Sjöqvist, V. Pasiskevicius and F. Laurell, *Narrow linewidth non-critically phase-matched volume Bragg grating OPO,* Mid-Infrared Coherent Sources (Barcelona, Spain, 2005), Mo6.

A10. L. Sjöqvist, M. Henriksson and O. Steinvall, *Simulation of laser beam propagation over land and sea using phase screens – a comparison with experimental data,* Proc. SPIE 5989, 59890D (2005).

A11. M. Henriksson, L. Sjöqvist and T. Uhrwing, *Numerical simulation of a battlefield Nd:YAG laser,* Proc. SPIE 5989, paper 59890I (2005).

A12. M. Henriksson, L. Sjöqvist, V. Pasiskevicius and F. Laurell, *Narrow Linewidth Near-Degenerate Optical Parametric Oscillation in Periodically Poled $LiNbO_3$ with Volume Bragg Grating Output Coupler,* Advanced Solid-State Photonics (Incline Village, USA, 2006), TuC4.

A13. M. Tiihonen, M. Henriksson, V. Pasiskevicius and F. Laurell, *Mid-IR ZGP-OPO Pumped by a Bragg Grating Line-Narrowed PPKTP-OPO*, Conference on Lasers and Electro-Optics (Long Beach, USA, 2006), CThO4.

A14. L. Sjöqvist and M. Henriksson, *Modelling thermo-optical effects in Nd:YAG lasers using a finite element method,* Northern Optics (Bergen, Norway, 2006), W28.

A15. M. Henriksson, L. Sjöqvist and O. Gustafsson, *Experimental study of mid-IR laser beam wander close to a jet engine exhaust,* Proc. SPIE 6397, 639709 (2006).

A16. V. Pasiskevicius, M. Tiihonen, B. Jacobsson, M. Henriksson, J. Hirohashi, C. Canalias and F. Laurell, *Optical parametric oscillators and amplifiers with periodically poled ferroelectrics*, Europhoton (Pisa, Italy, 2006). (Invited).

A17. M. Henriksson, M. Tiihonen, V. Pasiskevicius and F. Laurell, *ZGP Mid-Infrared Laser Source Pumped by Nearly-Degenerate PPKTP Parametric Oscillator*, Advanced Solid State Photonics (Vancouver, Canada, 2007), TuB22.

A18. L. Sjöqvist, O. Gustafsson, M. Henriksson and O. Steinvall, *Laser beam propagation close to jet engine plumes – performance implications on DIRCM system*, Threat Warning and Tracking in Atmospheric Turbulence (Ettlingen, Germany, 2007).

A19. M. Henriksson, L. Sjöqvist, M. Tiihonen, V. Pasiskevicius and F. Laurell, *Tandem OPO systems for mid-infrared generation using quasi phase-matching and volume Bragg gratings*, Proc. SPIE 6738, 673805 (2007).

A20. L. Sjöqvist, M. Henriksson, P. Jonsson and O. Steinvall, *Time of flight range profiling using time correlated single photon counting*, Proc. SPIE 6738, 67380N (2007).

A21. Ove Steinvall, Lars Sjöqvist, Markus Henriksson, and Per Jonsson, *High resolution ladar using time-correlated single-photon counting*, Proc. SPIE 6950, 695002 (2008).

A22. M. Henriksson, L. Sjöqvist, V. Pasiskevicius, F. Laurell, *Longitudinal mode structure of degenerate OPO with volume Bragg grating output coupler* Conference on Lasers and Electro-Optics (San Jose, USA, 2008), CTuY4.

A23. M. Henriksson, L. Sjöqvist, V. Pasiskevicius and F. Laurell, *Narrow bandwidth high power IR OPOs with volume Bragg gratings*, 17th International Laser Physics Workshop (Trondheim, Norway, 2008), 4.8.2 (Invited).

A24. M. Henriksson, L. Sjöqvist, G. Strömqvist, V. Pasiskevicius and F. Laurell, *Tandem PPKTP and ZGP OPO for mid-infrared generation*, Proc. SPIE 7115, 71150O (2008).

A25. M. Henriksson, L. Sjöqvist, D. Seiffer, N. Wendelstein and E. Sucher, *Laser beam propagation experiments along and across a jet engine plume*, Proc. SPIE 7115, 71150E (2008).

A26. L. Sjöqvist, C. Grönwall, M. Henriksson, P. Jonsson and O. Steinvall, *Atmospheric turbulence effects in single-photon counting time-of-flight range profiling*, Proc. SPIE 7115, 71150G (2008).

A27. C. Fureby, M. Henriksson, O. Parmhed, L. Sjökvist and J. Tegnér, *CFD Predictions of Jet Engine Exhaust Plumes*, 38th Fluid Dynamics Conf. and Exhibit, AIAA 2008-3727, (Seattle, USA, 2008).

A28. M. Henriksson, L. Sjöqvist, V. Pasiskevicius and F. Laurell, *Near-degenerate volume Bragg grating PPKTP OPOs in tandem OPO mid-IR sources*, Mid Infrared Coherent Sources (Trouville-sur-Mer, France, 2009), PO08.

A29. M. Henriksson, L. Sjöqvist, V. Pasiskevicius and F. Laurell, *Tandem optical parametric oscillator mid-infrared laser source*, Northern Optics (Vilnius, Lithuania, 2009), O-10.

A30. L. Sjöqvist, M. Henriksson, P. Jonsson and O. Steinvall, *Time-correlated single-photon time-of-flight range profiling and imaging*, Northern Optics (Vilnius, Lithuania, 2009), O-20.

A31. F. Kullander, P. Jonsson, M. Henriksson, G. Olofsson and P. Wästerby, *Short-range ultraviolet laser based standoff detection of chemical warfare agents*, Northern Optics (Vilnius, Lithuania, 2009), P2-6.

A32. O. Gustafsson, M. Henriksson and L. Sjöqvist, *Wall induced turbulence distortions of optical measurements*, Proc. SPIE 7482, 74820E (2009).

A33. M. Henriksson, L. Sjöqvist, V. Pasiskevicius, F. Laurell, *Cavity Length Resonances in a Singly Resonant Optical Parametric Oscillator with a Volume Bragg Grating*, Advanced Solid State Photonics (San Diego, USA, 2010), AMB21.

Technical reports

A34. T. Svensson, H. Larsson, L. Klasén, M. Henriksson, T. Carlsson, I. Nedgårds, D. Letalick, M. Elmquist, G. Carlsson and S. Cronström, "*Prov i Kvarn med passiva och aktiva optroniska sensorsystem,*" Technical report, FOI-R--0740--SE (2002).

A35. D. Letalick, P. Jonsson, T. Carlsson, M. Henriksson and H. Habberstad, "*Detection of buried land mines with laser vibrometry*," Scientific report, FOI-R--0909--SE (2003).

A36. O. Steinvall, L. Klasén, T. Chevalier, P. Andersson, H. Larsson, M. Elmqvist and M. Henriksson, "*Grindad avbildning - fördjupad studie,*" Scientific report, FOI-R--0991--SE (2003).

A37. A. Eriksson and M. Henriksson, "*Försök med OPO för generering av laserstrålning i våglängdsbandet 2-5 μm*," Technical report, FOI-R--1347--SE (2004).

A38. M. Henriksson, and L. Sjöqvist, "*Numerical simulation of a flashlamp pumped Nd:YAG laser*," Technical report, FOI-R--1710--SE (2005).

A39. A. Eriksson and M. Henriksson, "*Mid-IR laser for the LYSA system*," Technical report, FOI-R--1749--SE (2005).

A40. M. Henriksson, O. Gustafsson, L. Sjöqvist, "*Multi wavelength laser beam propagation close to a downscaled jet engine exhaust*," Technical report, FOI-R--2002--SE (2006).

A41. A. Eriksson, M. Henriksson, P. Jonsson, L. Sjöqvist, O. Steinvall, "*Ultrakorta laserpulser i verkanslaser och sensortillämpningar*," Technical report, FOI-R--2071--SE (2006).

A42. L. Sjöqvist, M. Henriksson, O. Gustafsson, M. Elmqvist, "*Laser beam progatation and active imaging experiments close to a jet engine plume*," Technical report, FOI-R--2529--SE (2008).

A43. M. Henriksson, D. Seiffer, L. Sjöqvist, R. Deron, H. M. A. Schleijpen, "*Study of jet engine plume phenomena on laser beam pointing and tracking*," FOI-R--2875--SE (2009).

Preface

The research forming this thesis has been performed at the Laser Systems Group, Division of Information Systems*, Swedish Defence Research Agency (FOI) in Linköping in collaboration with the Laser Physics group, Department of Applied Physics, KTH during 2005 to 2010.

The research has been done as part of my employment at FOI in projects sponsored by the Swedish Armed Forces and FMV, the Swedish Defence Materials Administration.

This thesis summarizes the work of five journal articles and a number of conference contributions and technical reports. The thesis consists of an introductory part, giving the background to the work and summarizing the results, and reprints of the five journal papers.

* Present name, earlier names have been Department of Laser Systems, Division of Sensor Technology and Department of Optronic Systems, Division of Sensor Systems.

Acknowledgements

First I would like to thank my supervisor Fredrik Laurell for accepting me as a Ph.D.-student and for encouraging me in my work. I would also like to thank my other two supervisors Valdas Pasiskevicius at KTH and Lars Sjöqvist at FOI. Valdas has been a great help in explaining the experimental results that sometimes surprised me. Lars has had to endure my visits to his room when I needed to discuss my results, and sometimes moan about the lack of results. He has also as project leader helped me focus my work on publishable research.

I am also grateful to Ove Steinvall, then head of the department, that encouraged me to start my Ph.D. studies. I am further thankful to the division heads at FOI, in order of appearance, Svante Ödman, Lena Klasén and Martin Rantzer, that have provided the financing for me to perform studies during working hours. I would also like to thank all my other co-workers at FOI in Linköping for providing a good working environment.

I would also like to thank Mikael Tiihonen for helping me with experiments in the KTH lab and Björn Jacobsson for valuable discussions on volume Bragg gratings. Many thanks to all former and present members of the laserphysics group for the welcoming acceptance at my visits to KTH and the good company at several conference trips. A special thanks goes to Jens Tellefsen that helped me with many practical details that are difficult to solve from a distance.

I would also like to acknowledge the Norwegian Defence Research Establishment for providing me with their OPO simulation software Sisyfos and Gunnar Arisholm for answering my questions on OPO simulations.

1. Introduction

1.1. Background

Transmission of electro-magnetic radiation through the atmosphere over longer distances is possible only in certain wavelength regions, often called windows, where the attenuation is low. These windows are evident in Figure 1-1 that shows the transmission through 10 km of air at different wavelengths. All of the wavelength ranges that have more than marginal transmission through the atmosphere can be used for optical sensors that detect radiation from objects at a distance. Below 2 μm the main natural radiation source is reflected sunlight, while the radiation emitted from hot objects dominates at longer wavelengths. In a military perspective sensors that track the infrared (IR) emission from hot objects are of especial interest, as they can be used as target seekers. Since their proliferation in the 1960s, man portable air-defence systems (MANPADs) using infrared seekers have been one of the largest threats against airplanes and helicopters in military and peace-keeping operations. Attacks against civilian aircraft have also occurred [1]. For this reason much effort has been placed on developing countermeasure systems against infrared seekers.

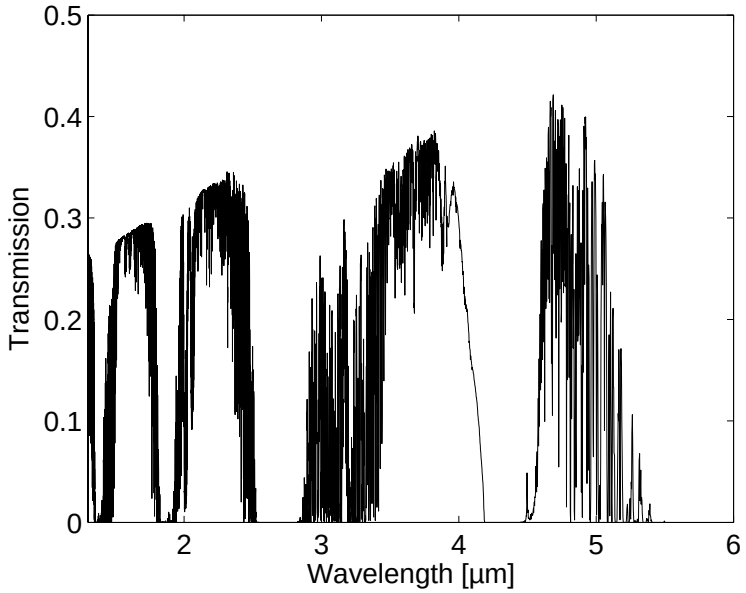

Figure 1-1. Transmission for 10 km propagation through subarctic winter atmosphere as calculated by MODTRAN [2].

Early model seekers can be defeated by ejecting hot flares that act as decoys and entice the seeker away from the infrared emission from the hot aircraft engine. To defeat modern seekers more potent countermeasures are needed. One way of deceiving the seeker is to shine a properly modulated laser on it. This method is called directed infrared countermeasures (DIRCM) and is the application that has motivated the laser source development reported in this dissertation. Some of the demands on the laser sources used in DIRCM applications are a wavelength in the seeker sensitivity range, high power with good beam quality and a pulse repetition frequency (PRF) higher than the seeker temporal bandwidth [3]. To be able to counter unknown threats it is advantageous to cover a large part of the infrared atmospheric transmission windows simultaneously. Especially important is the range 2 to 5 μm, which will be denoted the mid-IR range in this thesis. This is only one definition of

the mid-IR range, in other circumstances the whole 2 to 12 μm range may be included. As the DIRCM systems should be mounted on aircraft the laser sources need to be limited in size, maintenance requirements and power consumption.

Mid-IR laser sources that fulfil these demands are not readily available. A relatively recent review of mid-IR laser sources was provided by Godard [4]. In the future quantum cascade lasers have a potential of reaching the performance that is needed [5], and they are developing rapidly. Potentially they can be very small and have good wall plug efficiency. Gas lasers may give enough power at relevant wavelengths, but do not fulfil the engineering demands of the DIRCM application.

To this day the best laser sources that are available are near infrared solid state lasers with nonlinear optical wavelength conversion to the mid-IR using optical parametrical oscillators (OPO), see Figure 1-2. The first optical parametrical oscillator was reported in 1965 by Giordmaine and Miller using a $LiNbO_3$ crystal [6], and since then the field has evolved when new and better quality nonlinear crystals and pump lasers have become available. Nanosecond pulselength lasers are very suitable for pumping OPOs as this pulselength range provides a good compromise of peak power, pulse energy and average power.

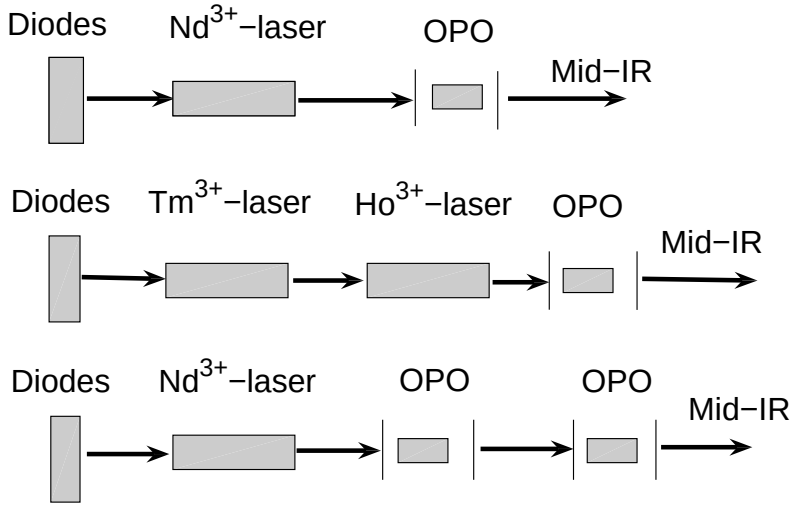

Figure 1-2. Some common schemes for generating mid-IR radiation using OPOs. The top one shows direct conversion from 1.06 μm to the mid-IR in an OPO. This is problematic at wavelengths longer than 4 μm due to absorption in nonlinear materials. The two lower schemes instead use non-oxide nonlinear materials that are transparent in the mid-IR, but absorb in the near-IR and thus need to be pumped at wavelengths longer than 2 μm. This pump can be generated either with a thulium-laser pumped holmium-laser (middle) or with a near degenerate OPO pumped at 1.06 μm.

Laser sources based on near infrared lasers and wavelength conversion using OPOs have been installed in DIRCM systems, but improvements in performance and especially in size and complexity are needed. The best developed diode pumped solid state lasers are the Nd^{3+}-lasers near 1.06 μm, and these have been used for conversion to wavelengths up to 4 μm with good performance. There are however so far no nonlinear optical crystals that can be used in an OPO for conversion from this wavelength to the important 4 to 5 μm wavelength range at high power levels. To reach these wavelengths an OPO with a nonlinear crystal that demand pump radiation at wavelengths longer than 2 μm are needed. There are two main possibilities to

produce this pump radiation, either by using a Ho^{3+}-laser [7,8], or by using an OPO to convert 1.06 μm laser radiation [9-14].

The solution of using an Nd-laser at 1.06 um and two OPOs in series to reach the 3.5 to 5 μm wavelength range was chosen for this project because of the greater flexibility, the availability and possible other uses of the pump laser. The realization of a narrow bandwidth type I quasi phase-matched (QPM) OPO using a volume Bragg grating (VBG) [15], showed a new possibility of creating a more efficient two stage OPO setup. The efficiency increase compared to the old method of using a type II bulk crystal OPO has three major reasons. The most important is that in the type II setup the signal and idler from the first OPO have different polarizations and consequently half of the energy from the first step is discarded, while in a type I setup signal and idler have the same polarization and can if their wavelengths are close enough together both be used for pumping the second OPO at the same time. The other two reasons are that QPM gives access to larger nonlinearity in the crystals and that it avoids Poynting vector walk-off that reduces the efficiency at tight focusing in birefringent phase-matching (BPM). At degeneracy the type I QPM interaction naturally has a very wide gain bandwidth and will in a traditional OPO cavity with dielectric mirrors produce wide bandwidth radiation that is unsuitable for pumping a second OPO. The doubly resonant nature of such an OPO may also cause unstable operation with large output power variation. To make the radiation useful a cavity that limits the feedback spectrum is required. Traditional methods of reducing the bandwidth with surface relief gratings and etalons introduce extra components in the cavity, causing unnecessary losses and lengthening the cavity, thus decreasing the efficiency. The use of a VBG output coupler produces narrow bandwidth feedback without any significant efficiency decrease. The term narrow bandwidth used here is as always relative. The topic is not single frequency laser sources. The spectral scale here is compared to dispersion in nonlinear crystals and the pump acceptance bandwidth in the second OPO in the tandem OPO system. Thus nanometre to sub-nanometre bandwidth is called narrow.

The main motivation for this work has been the development of a laser source for the DIRCM application, but our new improved method of producing narrow bandwidth laser radiation close to 2.13 μm and subsequently converting it to the mid-IR also has other applications. The most interesting alternative application is in medicine, where it has been shown that certain wavelengths, especially at 6.45 μm, can reduce the collateral damage from heating in laser surgery [16,17]. The mid infrared wavelength range is also very interesting for spectroscopy as many molecules have absorption lines in this region. Although the laser sources reported in this dissertation were not intended for spectroscopy it is possible that the developed techniques could be of interest also for spectroscopic laser sources.

1.2. Development of work

This thesis primarily discusses a new OPO scheme for converting 1.06 μm radiation from an Nd-laser to the 3.5-5 μm range. This scheme has also been patented [A4]. The main innovation in the concept is that a near degenerate quasi phase-matched OPO with a VBG output coupler is used to produce narrow bandwidth 2.13 μm radiation. The main focus of the work has been to study this type of OPO and the performance when pumping a second OPO with the output.

The work started by replacing the output coupling mirror in an earlier developed periodically poled lithium niobate (PPLN) OPO [A39], with a volume Bragg grating

resonant at 2008 nm [A9, A12, I]. When this proved to work as intended a new setup with higher pulse energy using a PPKTP crystal was built, that also allowed pumping of a ZGP OPO with the narrowband signal from the PPKTP OPO [II]. After this proof of concept new volume Bragg gratings were procured that allowed operation much closer to degeneracy and the concept of using both signal and idler to simultaneously pump a ZGP OPO to improve the overall efficiency was demonstrated [III]. Operation at higher PRF and efficiency optimization was reported in [A24]. After this goal was achieved the output from the PPKTP OPO was studied in more detail. Measurements of the spectrum at resolution high enough to resolve the longitudinal modes were performed [IV]. During the optimization process it was found that the output energy did not decrease monotonously with increasing cavity length. This has been reported earlier for doubly resonant cavities [18], but was unexpected in a singly resonant OPO and the cavity length resonances were studied in detail [V].

In parallel to the mid-IR source development the candidate has also worked on laser beam propagation from air-craft mounted laser systems by studying effects of laser beam propagation through jet-engine plumes [A15, A18, A25, A27]. The candidate has also been involved in laser radar research, especially systems for 3D-imaging [A1, A7], vibrometry [A5, A6], gated viewing [A36] and high range resolution range profiling using time-correlated single-photon counting [A20, A21, A26, A30].

1.3. Outline of the thesis

This thesis is based on the work that is reported in [I-V], included at the end of the thesis, and additional material previously published in conference proceedings and technical reports. After this introduction the next chapter will introduce the concepts of nonlinear optics that were needed for the work. Chapter 3 gives additional background and puts the work in perspective to efforts by other groups. The experimental results achieved are presented in chapter 4. Chapter 5 gives an introduction to the main application, DIRCM, and summarizes the work on beam propagation by the candidate. In chapter 6 a short description of the included papers is provided. Finally chapter 7 presents the main conclusions of the work and discusses some of the questions that still remain open.

2. Basic principles of nonlinear optics

The field of physics that describes propagation of electromagnetic radiation under conditions where the amplitude of the field influences the propagation is called nonlinear optics. This chapter contains a short introduction to a small part of the field that is relevant for the work in this thesis. For a more comprehensive discussion textbooks are recommended [19,20].

2.1. Basic nonlinear optics

A laser beam is an electromagnetic wave that is propagating in a well defined direction. The electromagnetic wave can be characterized by the rapidly varying electric field. The electric field can be described as

$$\mathbf{E}(\mathbf{r},t) = \hat{e}\frac{1}{2}A(\mathbf{r},t)e^{i(kx-\omega t)} + c.c. \tag{2.1}$$

where c.c. denotes complex conjugate and $\hat{e}$ is a unity vector defining the polarization direction of the field. It is assumed that the wavefront curvature radius is so large that $\hat{e}$ can be approximated to be transversal to the propagation direction of the laser beam, here defined as x in the coordinate system. The laser beam is assumed to be quasi-monochromatic, which means that the bandwidth of the variation of the amplitude A is small compared to the angular frequency ω of the optical wave. The amplitude of the electric field varies also in directions perpendicular to the propagation direction to define a limited beam. The beam from a high quality laser can often be approximated to have a circular Gaussian distribution, called the TEM_{00} mode. Diffraction effects cause the beam radius and divergence to change as the beam propagates, which also affects the peak intensity of the laser beam. It is to simplify calculations often assumed that the beam has an infinite extent perpendicular to the propagation direction. This is called the plane wave approximation. The measured quantities are in general optical intensity or the total optical power in the beam. The intensity of the laser beam can be calculated according to

$$I(\mathbf{r},t) = \frac{\varepsilon_0 nc}{2}\left|A(\mathbf{r},t)\right|^2, \tag{2.2}$$

where n is the index of refraction and c the speed of light. The power is determined by integrating the intensity over the cross-section of the beam.

Electromagnetic radiation passing through a crystal will apply a force on the electrons and ions in the material. The force causes primarily the electrons to oscillate and induces a time-varying electronic polarization in the material. For small electric field strength the material response in the frequency plane can be linearized to

$$\mathbf{P}_L(\omega) = \varepsilon_0 \boldsymbol{\chi}^{(1)}(\omega)\mathbf{E}(\omega), \tag{2.3}$$

where ε_0 is the permittivity of vacuum, $\mathbf{E}$ is the electric field and $\boldsymbol{\chi}^{(1)}$ is the linear susceptibility, which is described by a second-rank tensor. In an isotropic medium $\boldsymbol{\chi}^{(1)}$ is reduced to a scalar quantity $\chi^{(1)}$. Absorption in the material is neglected here, which makes $\chi^{(1)}$ a real quantity. The linear susceptibility is related to the index of refraction by $n = \sqrt{1+\chi^{(1)}}$. For larger field strengths, for example when the field is a high intensity laser beam, nonlinear contributions to the electronic polarization have to be taken into account. The total induced polarization can then be described by

$$\mathbf{P} = \varepsilon_0 \boldsymbol{\chi}^{(1)}\mathbf{E} + \varepsilon_0\left(\boldsymbol{\chi}^{(2)}\mathbf{E}^2 + \boldsymbol{\chi}^{(3)}\mathbf{E}^3 + ...\right) = \mathbf{P}^L + \mathbf{P}^{NL}, \tag{2.4}$$

where $\chi^{(m)}$ is the m:th order susceptibility tensor with rank m+1. An illustration showing the difference between linear and nonlinear polarization responses is given in Figure 2-1. Susceptibility tensors of even orders have non-zero components only in non-centrosymmetrical materials, so the second order nonlinearities that are the strongest are present only in certain crystals. Third order nonlinearities are, on the other hand, available in all materials, even in air.

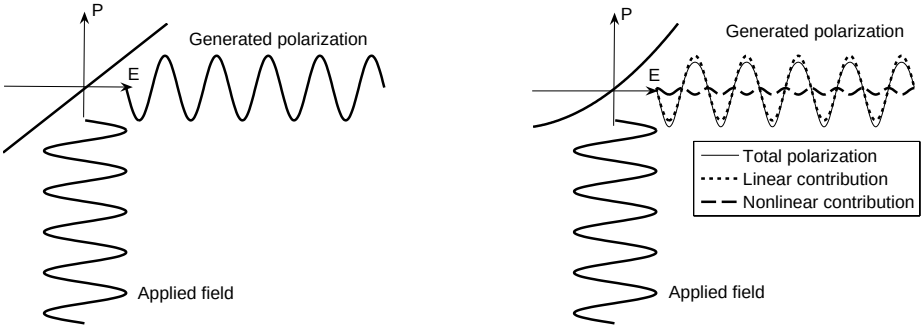

Figure 2-1. In the case of linear response the polarization will be proportional to the driving field (left), whereas when the material response is nonlinear the polarization will be distorted and contain contributions at harmonic frequencies.

The second order susceptibility $\chi^{(2)}$ is a third order tensor with rank 3 and 27 components. If all involved frequencies are far away from resonances in the material so that the loss can be neglected permutation or Kleinman symmetry holds. The second order susceptibility can then be contracted to a more easily handled 3×6 matrix, called *d*, and the polarisation $\mathbf{P}^{(2)}$ of the material due to second order nonlinear processes can be written according to

$$\begin{bmatrix} \left(P^{(2)}_{\omega_3}\right)_x \\ \left(P^{(2)}_{\omega_3}\right)_y \\ \left(P^{(2)}_{\omega_3}\right)_z \end{bmatrix} = 2\varepsilon_0 K \begin{bmatrix} d_{11} & d_{12} & d_{13} & d_{14} & d_{15} & d_{16} \\ d_{21} & d_{22} & d_{23} & d_{24} & d_{25} & d_{26} \\ d_{31} & d_{32} & d_{33} & d_{34} & d_{35} & d_{36} \end{bmatrix} \begin{bmatrix} \left(E_{\omega_1}\right)_x \left(E_{\omega_2}\right)_x \\ \left(E_{\omega_1}\right)_y \left(E_{\omega_2}\right)_y \\ \left(E_{\omega_1}\right)_z \left(E_{\omega_2}\right)_z \\ \left(E_{\omega_1}\right)_y \left(E_{\omega_2}\right)_z + \left(E_{\omega_1}\right)_z \left(E_{\omega_2}\right)_y \\ \left(E_{\omega_1}\right)_x \left(E_{\omega_2}\right)_z + \left(E_{\omega_1}\right)_z \left(E_{\omega_2}\right)_x \\ \left(E_{\omega_1}\right)_x \left(E_{\omega_2}\right)_y + \left(E_{\omega_1}\right)_y \left(E_{\omega_2}\right)_x \end{bmatrix}, \quad (2.5)$$

where each coefficient d_{ij} is dependent on the frequencies of the involved electrical fields. The two electromagnetic waves at frequencies ω_1 and ω_2 are here defined by their scalar electric field component in each polarization direction. Depending on material symmetries several coefficients d_{ij} can be zero or equal to each other, and in a material with total inversion symmetry all of them will disappear. The constant K is the degeneracy factor that is ½ if $\omega_1 = \omega_2$ and 1 if the waves have different frequencies.

To illustrate the generated material polarization we study the case where two plane electromagnetic waves with constant amplitude, but at different frequencies, overlap so that the incoming electric field can be described as

$$\mathbf{E}_{in}(x,t) = \hat{e}_1 \frac{1}{2}\left[A_1 e^{i(k_1 x-\omega_1 t)} + A_1^* e^{-i(k_1 x-\omega_1 t)} \right] + \hat{e}_2 \frac{1}{2}\left[A_2 e^{i(k_2 x-\omega_2 t)} + A_2^* e^{-i(k_2 x-\omega_2 t)} \right], \quad (2.6)$$

where the star denotes complex conjugate. The polarization generated by the second order nonlinearity in position $x = 0$ will then be

$$\begin{aligned}\mathbf{P}^{(2)}(x,t) = \frac{1}{2}\varepsilon_0 [& d_{eff}^{SHG_1} A_1^2 e^{i(2k_1 x-2\omega_1 t)} + d_{eff}^{SHG_2} A_2^2 e^{i(2k_2 x-2\omega_2 t)} \\ & + 2 d_{eff}^{SFG} A_1 A_2 e^{i((k_1+k_2)x-(\omega_1+\omega_2)t)} + 2 d_{eff}^{DFG} A_1 A_2^* e^{i((k_1-k_2)x-(\omega_1-\omega_2)t)} \\ & + d_{eff}^{RECT_1} |A_1|^2 + d_{eff}^{RECT_1} |A_2|^2 + c.c.].\end{aligned} \quad (2.7)$$

To make the equation more readable the direction vectors were omitted. The oscillation plane of the generated polarization is determined by the polarization planes of the incoming waves and by the different components of the *d*-tensor. In addition to the polarization planes the d_{eff} factors also depend on the involved frequencies. The different terms in the nonlinear polarization are generally denoted according to which frequencies are produced. The processes are called second harmonic generation (SHG), sum-frequency generation (SFG), difference frequency generation (DFG) and rectification (RECT). These notations are also used to label the d_{eff} factors in equation 2.7. Some of them are illustrated in Figure 2-2.

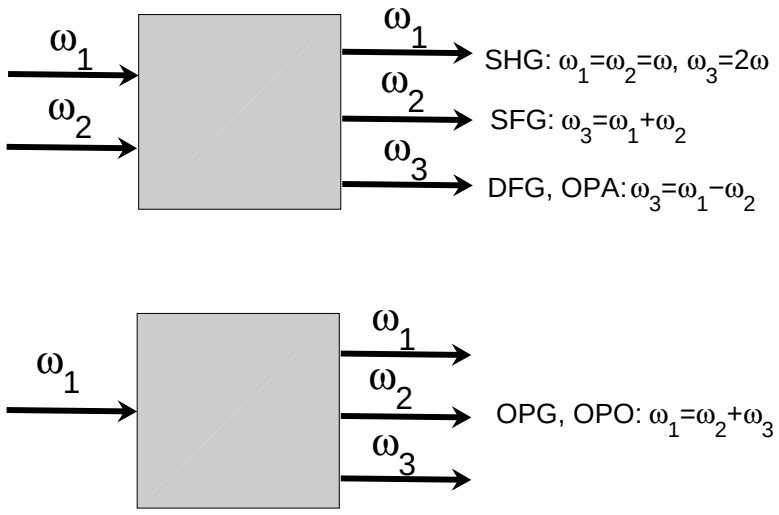

Figure 2-2. Common nonlinear optical processes from a three wave interaction.

The DFG process where the shortest wavelength beam (called pump) is much stronger than the longer wavelength input beam is so important that it usually treated separately and called optical parametric amplification (OPA). In a DFG process one photon in the pump beam will split into one photon of the frequency of the longer wavelength input beam and one photon of the difference frequency as depicted in Figure 2-3. In a parametric process the shorter wavelength generated (or amplified) beam is by convention called signal and the longest wavelength beam is called idler. In an OPA a weak (compared to the pump) seed at either the signal or idler wavelength is incident together with the pump beam. This seed is amplified by the parametric gain and at the same time the difference frequency is generated. Later on during propagation in the crystal the generated photons may interact with another

pump photon so that the signal and idler grow exponentially until the pump starts to be depleted. The process of applying only a pump beam and letting it amplify the vacuum field, generating frequencies that were not present initially, is usually called optical parametric generation (OPG) and is mostly used for ultrashort (picosecond or femtosecond) pulses as very high intensities are needed to reach efficient conversion. For nanosecond laser pulses and even continuous wave beams an optical cavity can be used to produce feed-back and amplify the generated beams in an optical parametric oscillator (OPO). OPOs are the main topic of this work and will be treated more thoroughly in section 2.3.

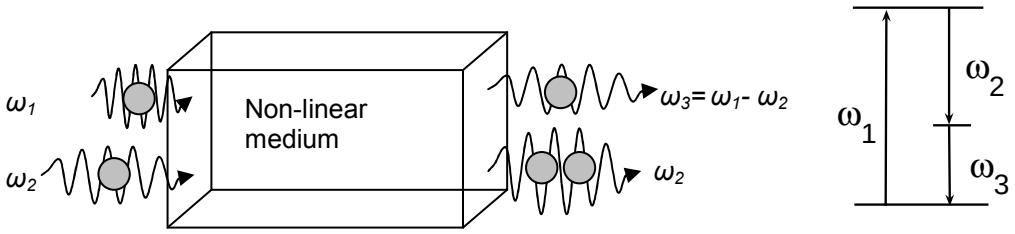

Figure 2-3. In a difference frequency generation process or a parametric amplification process one incoming pump photon at ω_1 and one signal photon at ω_2 will be converted to two photons at ω_2 and one photon at $\omega_3=\omega_1-\omega_2$.

In dielectric media, where there are no free charges and the magnetic permeability can be neglected, Maxwell's equations can be reduced to the wave equation with a nonlinear driving term

$$\nabla^2\mathbf{E}-\varepsilon_0\mu_0(1+\chi^{(1)})\frac{\partial^2\mathbf{E}}{\partial t^2}=\mu_0\frac{\partial^2\mathbf{P}^{NL}}{\partial t^2}. \tag{2.8}$$

This equation can in general not be solved analytically, but by using some assumptions a formulation more suited for calculations can be found. Assume that the electric field can be described by sums of a finite number of quasi-monochromatic plane waves propagating along the x-axis according to

$$\mathbf{E}(\mathbf{r},t)=\sum_j\hat{e}_j\frac{1}{2}A_{\omega_j}(\mathbf{r},t)\exp\left(i\left(k_jx-\omega_jt\right)\right)+c.c.. \tag{2.9}$$

The nonlinear contribution to the material polarization can in most cases be regarded as a small perturbation to the total polarization and be written as

$$\mathbf{P}^{NL}(\mathbf{r},t)=\sum_j\frac{1}{2}\mathbf{P}^{NL}_{\omega_j}(\mathbf{r},t)\exp\left(i\left(k_jx-\omega_jt\right)\right)+c.c., \tag{2.10}$$

where $k_j=n\left(\omega_j\right)\omega_j/c_0$ is the wave vector with $n(\omega)$ being the refractive index and ω the angular frequency of the optical wave. The frequency domain wave equation for propagation along the x-axis, obtained through Fourier transformation, is

$$\left(\frac{\partial^2}{\partial x^2}+\frac{\boldsymbol{\varepsilon}(\omega)\omega^2}{c_0^2}\right)\mathbf{E}\left(\mathbf{r},\omega\right)=-\mu_0\omega^2\mathbf{P}^{NL}\left(\mathbf{r},\omega\right), \tag{2.11}$$

where c_0 is the speed of light in vacuum and $\boldsymbol{\varepsilon}(\omega)=1+\boldsymbol{\chi}^{(1)}(\omega)$.

The wave equation can be used to deduce how the nonlinear polarization couples energy between electromagnetic beams at different frequencies. To simplify the equations we use the slowly varying envelope approximation (SVEA) where it is assumed that the variation of the field amplitude (due to linear and nonlinear processes) is small on the scale of the wavelength. This makes it possible to convert from a second to a first order derivative in the propagation direction in equation 2.11.

The result for a second order SFG process where radiation at frequencies ω_1 and ω_2 mix to generate radiation at frequency ω_3, using equation 2.5 to deduce the polarization, is a system of three coupled first order differential equations

$$\begin{aligned}\frac{\partial A_1}{\partial x} &= i\frac{\omega_1}{n_1 c} d_{eff} A_3 A_2^* e^{-i\Delta kx} \\ \frac{\partial A_2}{\partial x} &= i\frac{\omega_2}{n_2 c} d_{eff} A_3 A_1^* e^{-i\Delta kx} \\ \frac{\partial A_3}{\partial x} &= i\frac{\omega_3}{n_3 c} d_{eff} A_1 A_2 e^{i\Delta kx}\end{aligned}, \tag{2.12}$$

where $\Delta k = k_1 + k_2 - k_3$ is the phase mismatch. For all nonlinear processes energy conservation must apply so that the energies of generated and annihilated photons match. For a SFG process this condition is fulfilled when $\hbar\omega_3=\hbar\omega_1+\hbar\omega_2$.

For a SHG process with $\omega_1=\omega_2=\omega$ and $\omega_3=2\omega$ the system is further reduced to two nonlinearly coupled differential equations. At low efficiency where the intensity of the driving field can be assumed to be constant it collapses to one linear first order equation that can be solved analytically in a plane wave approximation. For this simplified case the second harmonic intensity is

$$I_{2\omega}(L) = \frac{\varepsilon_0 n_{2\omega} c}{2}\left|E_{2\omega}^2\right| = \frac{2\omega^2 d_{eff}^2 L^2 I_\omega^2}{\varepsilon_0 n_\omega^2 n_{2\omega} c^3}\operatorname{sinc}^2\left[\frac{\Delta kL}{2}\right], \tag{2.13}$$

where $\Delta k=k_{2\omega}-2k_\omega$ is the phase mismatch of the process, L is the length propagated in the nonlinear crystal, I_ω is the pump intensity, and n_ω and $n_{2\omega}$ are the refractive indices for the pump and the second harmonic fields, respectively.

2.2. Phase matching

It follows from equation 2.13 that second harmonic generation is most efficient when $\Delta k=0$. As the wave vector k is proportional to the refractive index this is a matching of the phase velocities of the pump and the generated wave. If the two beams propagate with the same phase velocity newly generated radiation will be in phase with the radiation that was generated in another part of the crystal and the amplitudes will add. If the velocities, on the other hand, are different the phases will alternately interfere constructively and destructively leading to very low conversion efficiency. In the general three wave SFG case the phase-matching condition is

$$\Delta k = 2\pi\left(\frac{n_3}{\lambda_3} - \frac{n_2}{\lambda_2} - \frac{n_1}{\lambda_1}\right) = 0, \tag{2.14}$$

that also can be interpreted as a momentum conservation condition since $p = \hbar k$. If nothing is done to ensure phase-matching the generated waves start to interfere destructively with waves generated at an earlier position after the coherence length

$$L_c = \left|\frac{\pi}{\Delta k}\right|, \tag{2.15}$$

which in general is a very short distance if proper care is not taken to minimize Δk. The requirement of zero phase-mismatch explains why we in general can reach appreciable conversion efficiency only for one of the possible nonlinear processes, even though we from equation 2.7 generate nonlinear polarization at several different frequencies. Because the efficiency of the other processes is so low, they can be

neglected when setting up the coupled differential equations (equation 2.12) for a numerical calculation.

At the same time as the phases are matched energy conservation

$$\Delta E = hc\left(\frac{1}{\lambda_3} - \frac{1}{\lambda_2} - \frac{1}{\lambda_1}\right) = 0, \tag{2.16}$$

has to apply. In a degenerate process, such as SHG, the only way of fulfilling both these conditions is to have equal refractive indices for the fundamental and harmonic waves.

In bulk materials, far from resonances where the material is absorbing, the refractive index is decreasing with increasing wavelength, i.e. normal dispersion. The dispersion is often modelled by the Sellmeier equation

$$n^2(\lambda) - 1 = \sum_i \frac{A_i \lambda^2}{\lambda^2 - \lambda_i^2}, \tag{2.17}$$

where λ_i are the resonance wavelengths and A_i their oscillator strengths. Most materials may be satisfactory modelled by two UV resonances and one far IR resonance. The result of this monotone dispersion curve is that the phase-matching conditions can not be fulfilled in the case where all waves have the same polarization. By using birefringent materials where the refractive index depends on the polarization it is often possible to fulfil the phase-matching condition by using the proper propagation direction in the crystal.

Birefringent crystals can be divided into uniaxial and biaxial crystals depending on the number of optic axes. For propagation along the optic axes all transversally polarized electromagnetic fields will sense the same index of refraction. In a uniaxial crystal the electric field can always be decomposed into one component that is polarized perpendicular to the optic axes and one orthogonal component in the plane spanned by the optic axes. The component that is polarized perpendicular to the optic axes will always sense the ordinary index of refraction n_o whatever the propagation direction is, and is called the ordinary beam. The other component, called the extraordinary beam, has a nonzero projection on the optic axes and senses an index $n_e(\theta)$ depending on the propagation angle according to

$$\frac{1}{[n_e(\theta)]^2} = \frac{\cos^2\theta}{n_o^2} + \frac{\sin^2\theta}{n_e^2}, \tag{2.18}$$

where θ is the angle between the optic axes and the propagation direction.

In a positive (negative) uniaxial crystal the extraordinary index is increasing (decreasing) with the angle θ from n_o for propagation along the optic axes to n_e for propagation perpendicular to the optic axes. As shown in Figure 2-4 this can be used to find a propagation direction θ where the extraordinary index for the fundamental wave is equal to the ordinary index for the second harmonic wave, thus compensating for the chromatic dispersion.

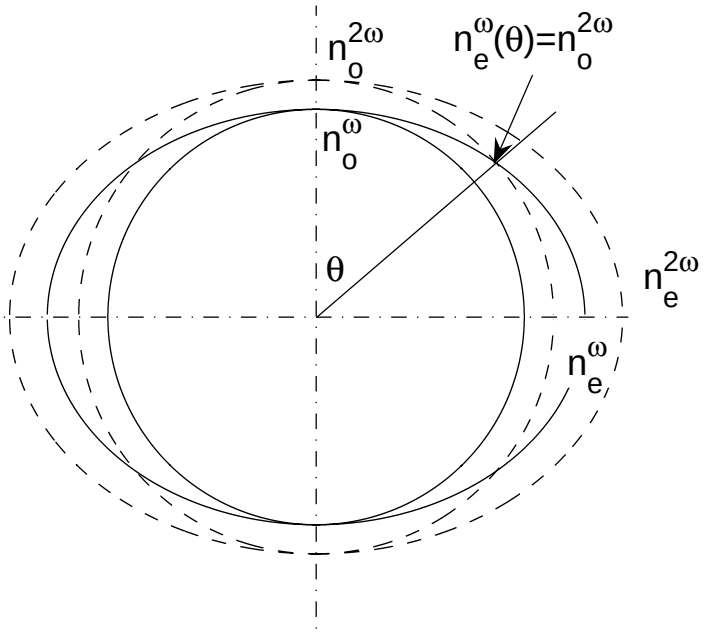

Figure 2-4. The index ellipsoids for a birefringent crystal. The picture shows how at angle θ the extraordinary index of refraction for the fundamental wave is equal to the ordinary index of the second harmonic.

In the case where propagation is not along one of the crystal axes the birefringence will lead to Poynting vector walk-off, where the extraordinary beam propagates at an angle ρ to the phase fronts, with ρ given by:

$$\tan\rho = -\frac{1}{n_e(\theta)}\frac{dn_e(\theta)}{d\theta}. \tag{2.19}$$

In a uniaxial crystal the walk-off can also be written as

$$\tan\rho = -\frac{1}{2}\left[n_e(\theta)\right]^2\left[\frac{1}{n_e^2}-\frac{1}{n_o^2}\right]\sin\left(2\theta\right). \tag{2.20}$$

Walk-off will reduce the spatial overlap between the ordinary and extraordinary beams and thus has a detrimental impact on conversion efficiency when using birefringent phase-matching (BPM). The effects of walk-off can be partly compensated by using two crystals oriented in a walk-off compensating scheme [21], as illustrated in Figure 2-5. Using twin crystals in a walk-off compensated scheme also has the advantage of removing beam translation during angle tuning [14].

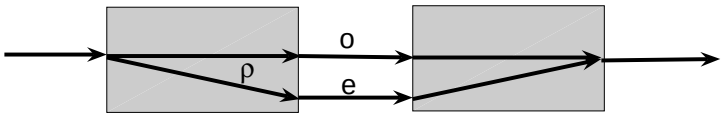

Figure 2-5. The extraordinary beam exhibits walk-off from the ordinary beam with the angle ρ when propagating in a birefringent crystal. This can be compensated with a second crystal inverted in the right manner.

Another way of compensating for the phase mismatch caused by the chromatic dispersion is quasi phase-matching (QPM), first introduced by Armstrong *et al.* in 1962 [22]. The principle of QPM is to change the phase of the generated radiation instead of adjusting the phases acquired through propagation. By changing the sign of the nonlinear coefficient d a phase shift of π is introduced. Quasi phase-matching

introduces a sign reversal every coherence length L_c so that d varies with a period $\Lambda=2L_c$ according to

$$d(z) = d_{ij}\,\mathrm{sign}\left(\cos\left(\frac{2\pi z}{\Lambda}\right)\right) = d_{ij}\sum_{m=-\infty}^{m=\infty} G_m e^{ik_m z}$$
$$G_m = \frac{2}{m\pi}\sin\left(\frac{m\pi}{2}\right), \qquad k_m = \frac{2\pi m}{\Lambda} \tag{2.21}$$

This modulation of d adds an extra vector in the phase space. If the period is chosen correctly, i.e. two coherence lengths, the grating phase vector cancels the phase mismatch for order m=1 according to

$$\Delta k - k_{QPM} = 0\,. \tag{2.22}$$

In certain cases the phase mismatch is so large that periods short enough are not possible to manufacture and higher orders of m have to be used, even though the power efficiency is proportional to $1/m^2$. Only odd orders m can be used for QPM if the duty cycle is 50 %, as even orders would introduce the phase shift at zero generated power. This is also evident from the expression for the G_m coefficient, which is zero for even orders.

By inserting the Fourier expansion of d into the coupled wave equations using the same assumptions as in equation 2.13 the following efficiency for second harmonic generation with QPM is found:

$$I_{2\omega}(L) = \frac{\varepsilon_0 n_{2\omega} c}{2}\left|E_{2\omega}^2\right| = \ldots = \frac{2\omega^2 I_\omega^2}{\varepsilon_0 n_\omega^2 n_{2\omega} c^3}\left[\left(\int_{-L/2}^{L/2} d_{ij}\sum_{m=-\infty}^{m=\infty} G_m e^{ik_m z}\right)e^{-i\Delta k z}dz\right]^2 =$$
$$\frac{2\omega^2 I_\omega^2}{\varepsilon_0 n_\omega^2 n_{2\omega} c^3} L^2 d_{ij}^2\left(\frac{2}{m\pi}\right)^2 + \text{ osc. terms, for } \Delta k = k_m. \tag{2.23}$$

The generated intensity is equal to the phase matched case with $d_{QPM} = 2d_{ij}/(m\pi)$. The Fourier terms that are not matched to the phase mismatch will only cause an oscillation in power with crystal length. An illustration of the power growth for the different phase matching cases is shown in Figure 2-6. Despite the $(2/\pi)^2$ reduction in efficiency when using QPM it is often more efficient than birefringent phase matching as polarization combinations with higher d_{ij}, that are not accessible with birefringent phase matching, can be used. Normally the crystal directions are defined so that d_{33} is the largest component and all electric fields should thus be aligned along the z-axes of the crystal. An additional advantage of QPM is that the propagation direction can always be selected to be along one of the principal crystal axis so that walk-off is avoided.

Ferroelectrics are the most commonly used materials for QPM. They have a spontaneous electronic polarization. By applying a strong electric field this polarization can be inverted by movement of ions between two positions in the crystal lattice. At the same time the sign of the nonlinear optical coefficient d_{eff} will change. By fabricating a periodic pattern of electrodes on one face of a single domain crystal and applying high voltage a permanent 180° domain grating suitable for quasi phase-matching can be produced [23,24]. This process is called periodic poling.

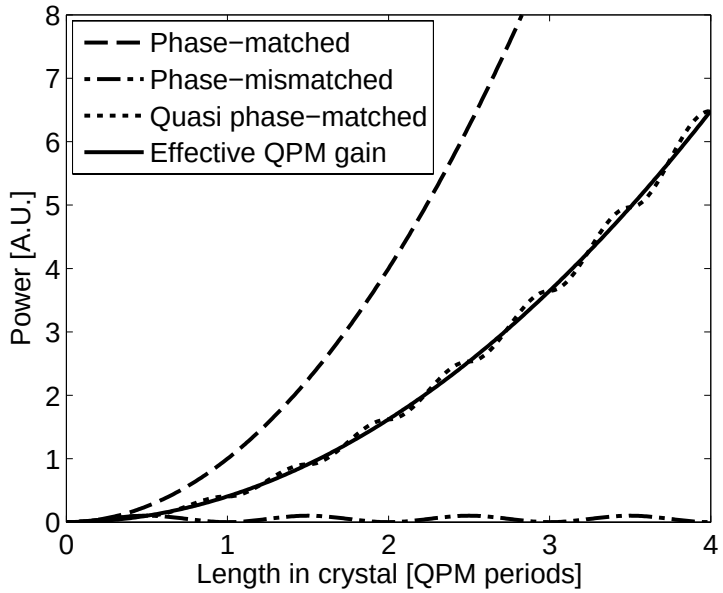

Figure 2-6. Second harmonic intensity with different types of phase-matching assuming equal d_{eff}.

A distinction is made between two polarization combination possibilities of phase-matching. If the two lower frequency beams, that are input beams in an SFG process or are generated in a parametric process, have the same polarization the scheme is denoted type I phase-matching. If, on the other hand, the two low frequency, and hence longer wavelength, beams have different polarizations the phase-matching is of type II. One point to be made is that the wavelengths for the two polarizations cross at the angle where a parametric process produces degenerate frequencies for type II interaction (Figure 2-7), but for type I interaction phase-matching is possible only on one side of the degenerate angle (Figure 2-8). To be noted is also that the effective nonlinearity varies as a function of propagation angle. There is a possibility that even if the interaction is phase-matched d_{eff} may be zero because of unfortunate material symmetries. This is, for example, the case for type I interaction in KTP [25].

Perfect phase-matching is achieved for only one specific wavelength combination. If one of the three wavelengths involved in a second order nonlinear process changes, at least one of the other wavelengths has to adapt to comply with energy conservation. This wavelength change will cause a phase mismatch. The frequency ranges where $|\Delta kL| < C$ are called acceptance bandwidths. The constant C can be chosen in different ways, but one definition is to use the first zero of the sinc^2-function that appears in solutions of the coupled wave equations using the non-depleted pump approximation (2.13), so that $2C$=0.886×2π [26]. The maximum change of ω_j when ω_l is adapted is in a linear approximation limited by

$$C > L\left|\left(\frac{\partial k_j}{\partial \omega_j} - \frac{\partial k_l}{\partial \omega_l}\right)\Delta\omega_j\right| = L\left|\left(\frac{1}{v_{g,j}} - \frac{1}{v_{g,l}}\right)\Delta\omega_j\right| = \left|t_{w,jl}\right|\Delta\omega_j . \qquad (2.24)$$

The acceptance bandwidth can thus be defined as

$$\Delta\omega_{jl} = \frac{2C}{\left|t_{w,jl}\right|}, \qquad (2.25)$$

where allowing the mismatch to go from $-C$ to C causes the factor 2. This result shows that the acceptance bandwidths are related to the temporal walk-off of the involved beams [27].

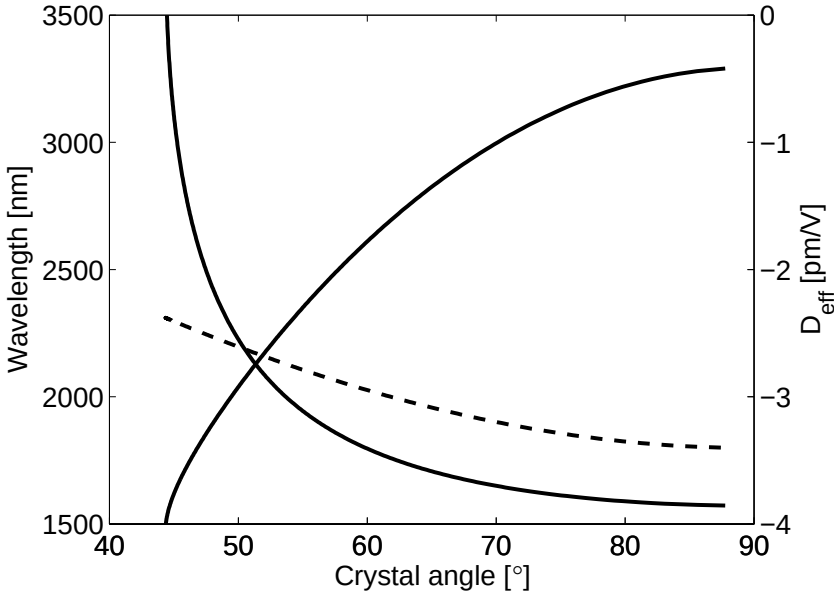

Figure 2-7. Phase-matching curves for type II interaction in KTP with a 1064 nm pump beam (solid). The effective nonlinearity for the relevant propagation angle and polarization combination (dashed).

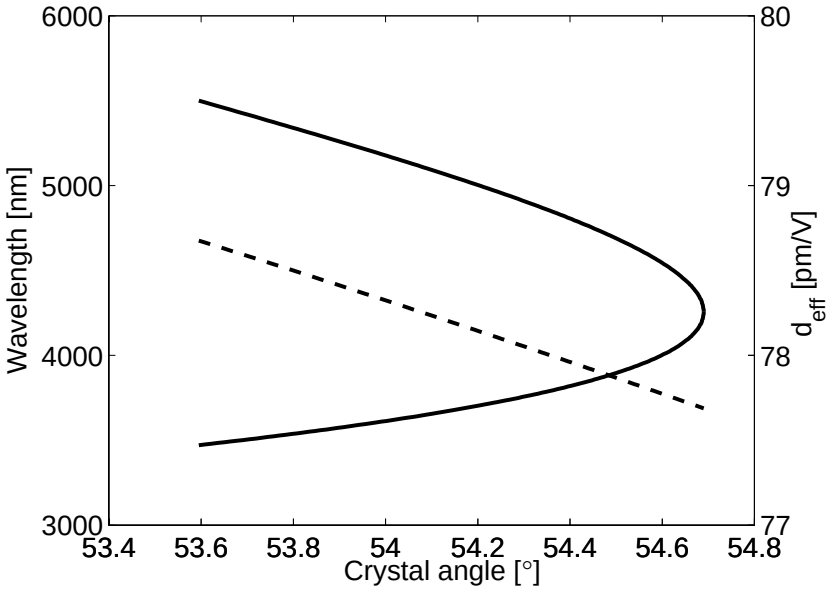

Figure 2-8. Phase-matching curves for type I interaction in ZGP with a 2128 nm pump beam (solid). The effective nonlinearity for the relevant propagation angle and polarization combination (dashed).

It is interesting to study the bandwidth in the case of type I and type II phase matching for degenerate OPOs. Let us fix the pump frequency and choose perfect phase-matching. In type II phase matching the generated waves then have different polarizations, and thus in a birefringent material different group velocities. The temporal walk-off is thus finite and the bandwidth generated from the OPO relatively small. In a type I OPO the two generated waves are truly degenerate, and the temporal

walk-off exactly at degeneracy disappears. To find the much larger acceptance bandwidth in this case it is necessary to include higher order terms in the Taylor expansion of the phase mismatch in equation 2.24. This explains the very large bandwidths generated in a type I OPO close to degeneracy.

If the pump is multi longitudinal mode the pumping efficiency will decrease with increasing bandwidth. Often an acceptance bandwidth is defined to give an indication on the acceptable pump linewidth for the specific material and pumping wavelength with a fixed signal wavelength. The full width half maximum (FWHM) acceptance spectral width $\Delta\lambda$ can be defined so that $\mathrm{sinc}^2\left(\Delta kL/2\right)=0.5$ for $\lambda=\lambda_0\pm\Delta\lambda/2$. The phase mismatch is calculated by a Taylor expansion of the refractive index around the phase matching wavelength, neglecting changes in the signal and idler wavelengths due to pump tuning, so that

$$\Delta k=\frac{2\pi}{\lambda}\frac{\partial n}{\partial\lambda}\bigg|_{\lambda=\lambda_0}\Delta\lambda+\frac{2\pi}{\lambda}\frac{\partial^2 n}{\partial\lambda^2}\bigg|_{\lambda=\lambda_0}\Delta\lambda^2, \tag{2.26}$$

where the second term in general is small compared to the first. To define a material parameter the length-bandwidth product $\Delta\lambda L$ is the value used. For example, considering a ZGP OPO pumped at 2128 nm the acceptance bandwidth is 6.5 nm×cm. Similar relations can be used to calculate the sensitivity to a certain parameter in a fixed wavelength nonlinear process, e.g. an OPO with intracavity wavelength selective elements, second harmonic generation or difference frequency generation. Important parameters include wavelength, temperature and crystal angle.

2.3. Optical parametric oscillators

When a nonlinear crystal is placed in a cavity and pumped by a strong laser beam the parametric fluorescence is fed back to the crystal and amplified, as illustrated in Figure 2-9. This device is the optical parametric oscillator (OPO). OPOs pumped by nanosecond laser pulses are an established technology that is used in many applications. Several reviews describing their physics and applications have been presented, although there is so far no complete analytical theory [28,29].

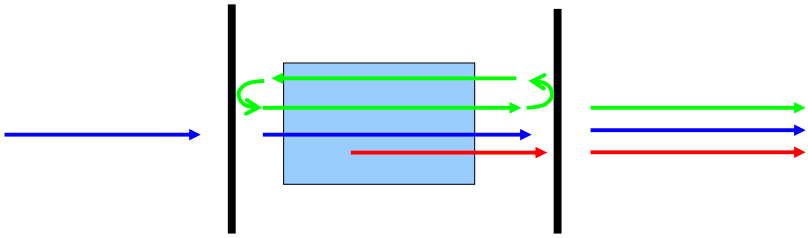

Figure 2-9. Illustration of a simple OPO consisting of a nonlinear crystal surrounded by two mirrors. The OPO is singly resonant as only the signal is resonated in the cavity, and the idler is transmitted out at each roundtrip in the cavity. As the output coupler transmits the pump power remaining after one pass through the nonlinear crystal this is a single pass pump configuration.

If the parametric process is phase matched the amplification during one round-trip may exceed the cavity losses. When using nanosecond laser pulses for pumping the peak intensity is in general so high that there is a large net gain. The signal and idler will thus experience exponential growth. This will continue either until the end of the pump pulse or until the conversion efficiency reaches so high values that the pump is depleted. When the signal and idler reaches intensities of the same order as the pump

the nonlinear conversion may change direction, producing radiation at the pump wavelength by back conversion.

In accordance with a laser the pump level where the gain equals the cavity losses is called the threshold for the continuous wave (cw) OPO operation. In a pulsed OPO a peak power only slightly above this level will never have time to produce a measurable output before the pump pulse ends. The threshold of the pulsed OPO is therefore usually defined as the pulse energy that is needed to produce a measurable output. The growth rate of the generated output above the threshold is called the slope efficiency, whereas conversion efficiency denotes output power divided by pump power.

The single pass parametric power gain in the nonlinear crystal is [30]

$$G = \Gamma^2 L^2 \frac{\sinh\left(\sqrt{\Gamma^2 - \frac{\Delta k^2}{4}} L\right)}{\left(\Gamma^2 - \frac{\Delta k^2}{4}\right) L^2}, \tag{2.27}$$

where L is the crystal length, Δk is the phase mismatch and Γ is the parametric gain factor given by

$$\Gamma^2 = \frac{2\omega_s \omega_i d_{eff}^2 I_P}{\varepsilon_0 n_p n_s n_i c^3}. \tag{2.28}$$

In the gain factor the quotient $d_{eff}^2 / \left(n_p n_s n_i\right)$ can be identified. This expression contains all material dependence and is thus often called the nonlinear figure of merit for the material.

The losses in the OPO cavity originate from absorption, scattering and parasitic reflections in the cavity, but primarily from the finite reflections of the cavity mirrors. In fact for the OPO to produce any output either the signal, the idler or both beams must have some fraction transmitted out of the cavity to generate the desired beam. Depending on if the cavity mirrors are reflecting both or only one of the signal and idler waves the OPO is called doubly or singly resonant (DRO or SRO), respectively. The double feedback in the DRO gives a much lower threshold than in the SRO. Each resonant wave in the OPO however has to fulfil the cavity conditions for longitudinal modes

$$2L = m\lambda_m, \tag{2.29}$$

where m is an integer number and $2L$ is the roundtrip optical path length of the cavity with the factor 2 being a result of the passage back and forth in a linear cavity. The normal case is that the separation of the longitudinal modes is so small that many modes fit within the gain bandwidth of the OPO. In the DRO case there will be two waves that are resonant in the cavity, and as their wavelengths are coupled by energy conservation only certain cavity lengths allow DRO operation if a single frequency pump is used. If the resonance conditions are not fulfilled the phases of the three beams will not have the same relation on successive passes in the nonlinear crystal and efficient conversion is inhibited. The instability is less severe with a multimode pump because of the rapidly varying phase of the pump beam [31]. For continuous wave (CW) operation active cavity length control is required for stable operation because of thermal instabilities, but this may be motivated by the significantly reduced threshold. Another reason to use DROs is that for near degenerate operation it

can be difficult to distinguish between the signal and idler at the cavity mirrors. In a free running near degenerate DRO the gain bandwidth is in general so wide that there are always some combinations of longitudinal modes that fulfil energy conservation, and active cavity length control is thus not needed for broadband operation. In the SRO the non-resonated wave is free to take any wavelength that fulfils energy conservation and there are no restrictions on cavity length.

Another distinction between different cavity types is if the pump passes only once through the crystal, single pass pumping, or if the pump remaining after the first pass is reflected back to pass a second time through the crystal to provide amplification also in the opposite direction, so called double pass pumping. Double pass pumping will reduce the threshold and increase the efficiency but may cause deterioration of the beam quality.

The simplest cavity configuration is the linear SRO cavity consisting of only the nonlinear crystal and two mirrors, see Figure 2-9. The incoupling mirror transmits the pump and reflects the signal, and the outcoupling mirror is usually partially reflecting for the signal and transmits the pump and the idler. The mirrors can be flat or curved to match the resonant mode to the pump waist. More complicated folded or ring-formed cavities involving several mirrors are also possible. The ring OPO has the advantage of ensuring that no pump radiation is reflected back to the laser, thus removing the need for an optical isolator. In addition the ring cavity can avoid having the resonated signal pass through the crystal without a co-propagating pump beam and thus reduces potential back-conversion to the pump wavelength. This is especially important in a DRO where both signal and idler are resonated. The main disadvantage of the ring cavity is that it generally becomes longer than a standing wave cavity. It may also be more difficult to align.

The theoretical threshold of singly resonant optical parametrical oscillators, for single and double passing of the pump, was derived by Brosnan and Byer [32]. The threshold energy can vary between a few microjoules [33] and several millijoules depending on nonlinear crystal, mirror reflectivities, wavelengths, focusing conditions and other parameters of the pump pulse and of the OPO cavity. The maximum efficiency of an OPO with a Q-switched wide focus Gaussian pump beam, where the nonlinear crystal is shorter than the Rayleigh length, and plane mirrors was calculated by Bjorkholm and is 71 % in the singly resonant case [34]. Parameters preventing 100 % efficiency include energy in the low intensity spatial wings of the Gaussian beam [35], and the OPO build-up time. For each OPO setup there will be a pump pulse energy that produces optimum efficiency, although this may be less than the theoretical limit. The primary goal when designing an OPO should be to get the optimum efficiency at the maximum pump power. The main design parameters are the output coupling and the pump intensity, regulated by the beam waist diameter. The pump intensity is ultimately limited by the crystal damage threshold, but the efficiency may start to decrease already at lower intensities due to back-conversion through sum frequency generation of signal and idler. In high average power devices additional difficulties are introduced by thermal effects due to absorption in the nonlinear crystal.

The wavelengths generated by an OPO are determined by energy conservation and phase matching, as discussed in section 2.2. One advantage of an OPO is that the phase matching conditions can be changed and thus the OPO is a tuneable source of laser radiation. Basically every parameter that influences the index of refraction of the

nonlinear medium can be used for tuning. The most common parameters to use are the crystal angle or temperature. Selection of the wavelength can also be made by fabrication of different QPM domain grating periods. In addition it is possible to vary the signal and idler wavelengths by pump tuning where the crystal parameters are constant and the wavelength of the pump is changed instead. An example depicting how the wavelengths change with temperature and domain grating period in periodically poled $LiNbO_3$ (PPLN) is shown in Figure 2-10. Explanations for the mismatch between theoretical and experimental data could include temperature measurement errors, period offsets in fabrication and inaccuracy in the refractive index model.

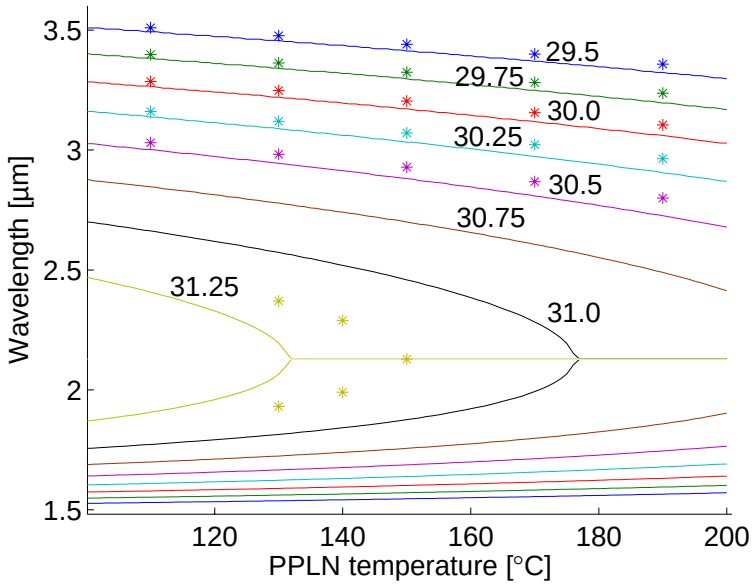

Figure 2-10. Signal and idler wavelengths for a PPLN OPO depending on temperature. The solid curves represent theoretical tuning curves and are labelled by the domain grating periods in micrometer. The stars show experimental data [A39].

3. Mid infrared optical parametric oscillators

3.1. Nonlinear materials for mid-IR generation

There are several parameters that have to be taken into consideration when selecting nonlinear crystal. They include, for example, transparency range, damage threshold, thermal conductivity, phase matching possibility, mechanical hardness, nonlinear figure of merit, crystal availability and price.

For conversion from 1 μm to the shorter wavelength part of the mid-infrared spectral range from 2 to approximately 4 μm there are a number of oxide based crystals that are possible to use. The most common ones are congruently grown $LiNbO_3$ (LN) and $KTiOPO_4$ (KTP). LN is mainly used with periodical poling (PP) for quasi phase matching [36], whereas KTP is used both in bulk form with BPM and as PPKTP [23,24]. PPLN is the dominating crystal for low peak power applications as it has wide transparency and high gain (d_{33}=25.2 pm/V [37]). Long crystals lengths (up to 50 mm) are available, but PPLN has low damage threshold. The pulse energy is also limited by the aperture and PPLN crystals thicker than about 1 mm are difficult to pole due to a high coercive field, although thicker samples exist [38]. PPLN OPOs generally have to be operated at elevated temperatures to avoid damage caused by the photorefractive effect. Doping with a few percent of MgO reduces the sensitivity to photorefractive effects [38]. An alternative to PPLN with better resistance to photorefractive effects is periodically poled stochiometric lithium tantalate (PPSLT) [39]. PPSLT however still has low optical damage threshold, and also lower nonlinearity.

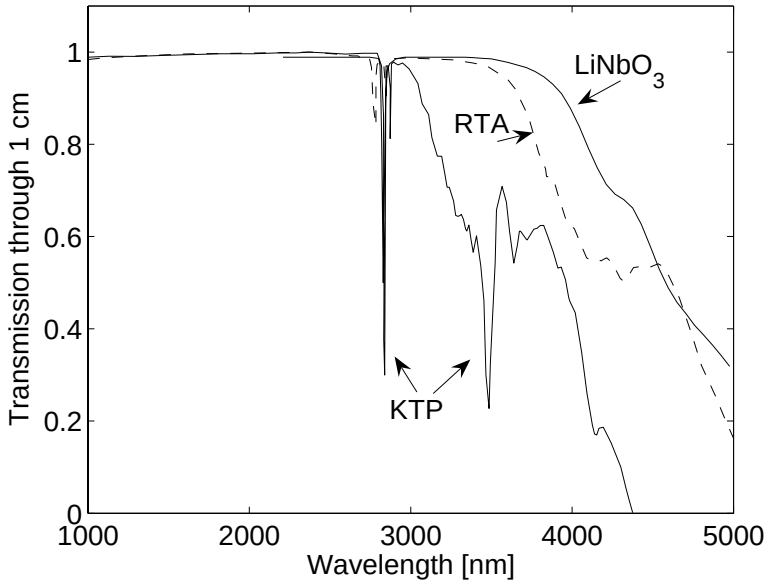

Figure 3-1. Transmission curves for $KTiOPO_4$, $RbTiOAsO_4$ and $LiNbO_3$ [25].

KTP has a higher damage threshold than LN, but has a shorter wavelength absorption cut-off around 3 μm. The coercive field for periodic poling of KTP is also lower than that of LN and thus poled crystals as thick as 3 mm suitable for high energy applications has been fabricated [40]. For birefringent phase matching in KTP the nonlinear susceptibility component used is d_{24}=3.9 pm/V. Using QPM it is possible to access the stronger nonlinear coefficient d_{33}=15.3 pm/V [41]. Alternatives

to KTP are its isomorphs $KTiOAsO_4$ (KTA), $RbTiOPO_4$ (RTP) and $RbTiOAsO_4$ (RTA), where the arsenates are especially interesting for IR applications because of their longer transparency range [42]. Transmission curves for KTP, RTA and LN are given in Figure 3-1 for the region 1 to 5 μm [25].

At wavelengths longer than 4 μm the situation is more complicated. The oxide materials are limited by absorption, and although PPLN OPOs can be operated at longer wavelengths [43], they are not a good alternative for generating high average powers in the 4 to 5 μm wavelength range. Several non-oxide materials have been used for 1 μm pumped OPOs to the mid-IR, but only at low PRF and hence low average power. These experiments were recently reviewed [44]. The recently developed crystal $CdSiP_2$ can be used for conversion from 1 μm to 6.2 μm and show promise for high average power operation [45,46], but cannot be phase-matched for shorter wavelengths. Pumping of OPOs for generation of mid-IR radiation thus has to be done at wavelengths longer than 1.5 μm and in most cases even longer than 2 μm. The materials $AgGaSe_2$ (AGSe) and $AgGaS_2$ (AGS) that were used in early experiments [47-50], suffer from low damage thresholds and poor thermal conductivity and were not suitable for high repetition rate OPOs. The chalcopyrite $ZnGeP_2$ (ZGP) was first suggested for nonlinear optics in 1971 [51]. When high quality ZGP became available in the late 1990ies it almost totally displaced the other crystals. ZGP has high nonlinearity (d_{eff}=75 pm/V [20]), good thermal conductivity and acceptable damage thresholds. The short wavelength transmission cut-off is near 2 μm, as seen in Figure 3-2, but the exact position and shape is sensitive to impurities in the crystal and the growth is thus very critical [52]. ZGP will be further discussed in section 3.3.

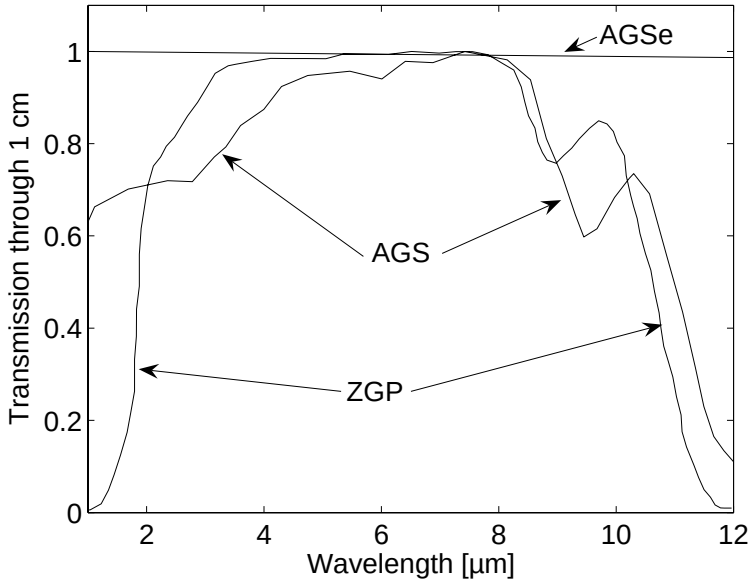

Figure 3-2. Transmission graphs for ZGP, AGS and AGSe [25].

Other less frequently used nonlinear materials for the mid-infrared include CdSe, GaSe and $CdGeAs_2$ (CGA). CdSe has been used for OPOs [53], whereas the crystal quality of the soft layered GaSe has not allowed OPO operation. CGA has an extremely high figure of merit, 57 times that of PPLN, but the transparency is not that good and OPO operation has only been shown with 4.8 μm pumping [54].

Several semiconductor materials such as GaAs, GaP and ZnSe show high nonlinearities, large transparency ranges, good damage thresholds and high thermal conductivity. They, however, have no birefringence and are not ferroelectric and can hence not be periodically poled. QPM experiments have been done with stacks of thin material sheets [55], but problems with slicing the materials thin enough and low loss bonding of the stacks limit the efficiency for the short periods needed in mid-IR OPOs. In the last few years progress has been made on orientation patterned (OP) molecular beam epitaxial growth of GaAs [56,57], and hybrid growth for thicker samples [58]. Good OPO performance has already been achieved [59], showing promise for future availability of a QPM material for longer wavelengths. GaAs has an absorption band edge at 0.9 μm but high two-photon absorption limits pumping with nanosecond laser pulses to above 1.8 μm. GaP on the other hand has its transparency edge at 0.5 μm and pulsed pumping of GaP by Nd^{3+}-lasers at 1.06 μm could become possible in the future, but so far QPM of GaP has been shown only by stacking of plates for DFG to THz frequencies [60]. Shorter periods than possible with wafer bonding will be needed for mid-IR OPOs and orientation patterned growth of GaP is at least theoretically possible.

3.2. Prior art 2 μm laser sources for OPO pumping

There have been a number of studies on OPO pumping at, or above, 2 μm reported in the literature. Examples of direct pumping by lasers include, but are not limited to, Ho^{3+}-lasers pumped by Tm-YLF lasers [7] and Tm-fiber lasers [8]. The reason for this double laser scheme is that Ho^{3+} lacks absorption bands that coincide with the emission spectra from commercially available efficient diode lasers. Thulium lasers can on the other hand be pumped at 790 nm with a two for one photon scheme in a cross-relaxation process and generates 1.9 μm pump radiation for a Ho^{3+}-laser with good efficiency. High power diodes at 1.9 μm are being developed [61], and directly diode pumped Holmium-lasers may be an alternative in the future. Direct pumping of a ZGP OPO by a bulk Tm^{3+}-laser is not advisable because of material absorption, but for OP-GaAs OPOs this may be an alternative. Another option is pumping with a Cr:ZnSe laser, that has the interesting emission band from 2.1-2.8 μm, making pump tuning of the mid-IR OPO possible [58]. Cr:ZnSe lasers can not be Q-switched but need to be pumped by a pulsed laser near 1.9 μm for gain switching which makes a complex system. One advantage of pump tuning over angle tuning of an OPO is that the position and angle of the generated radiation does not change with the wavelength, something that may be important for long range transmission. Recent development of gain switched Tm-fiber lasers and fiber power amplifiers has made direct fiber laser pumping of a ZGP OPO possible [63], but the needed fiber sources are complicated multi stage devices. Pumping of a OP-GaAs OPO using a Q-switched Tm:Ho:fiber laser with bulk optics and a VBG for bandwidth narrowing has also recently been demonstrated [64].

The best developed solid-state lasers are Nd^{3+}-lasers that are used for applications like lidars and material processing. By using an OPO the 1.06 μm wavelength of these lasers can be converted to the 2 μm range suitable for pumping ZGP. The standard scheme has been to use a type II bulk KTP OPO with birefringent phase-matching. Different configurations such as linear cavities with a single crystal [8], with walk-off compensated crystal pairs [10], ring cavities [11], polarization rotating cavities [12] and intracavity OPOs [13] have been demonstrated. By changing the angles of the

crystals in a walk-off compensated pair of KTP crystals pump tuning is possible without realigning the second OPO [14].

Because of the higher nonlinearities and the absence of walk-off QPM OPOs are very interesting alternatives. Near degenerate OPOs using QPM crystals, however, have a very wide gain bandwidth. For example, a bandwidth of 210 nm (FWHM) around degeneracy was measured in a PPKTP OPO pumped at 1064 nm in a reference measurement [III]. Solutions to this problem include pumping with a 1.3 μm Nd:YAG laser to generate a signal at 2.12 μm without being close to degeneracy [65], and type II QPM with a polarization rotating cavity, that uses a polarization combination with a smaller nonlinear coefficient [66].

An alternative and straightforward scheme for overcoming the wide bandwidth in a type I OPO is to make the cavity spectrally selective to reach threshold only for a small bandwidth. Traditional methods use etalons, diffraction gratings in Littman and Littrow configurations and birefringent filters [32,67]. All of these methods introduce extra loss at the desired wavelength, thus the threshold is raised and the slope efficiency decreases. By using a low efficiency, low power OPO to generate a beam with good spatial and spectral quality and then amplifying it in an OPA a good high energy pump source can be obtained, as shown by Saikawa *et al.* with a pair of MgO:PPLN crystals [68]. It should also be possible to use the low power beam to seed an OPO.

The interest in type I OPOs operating very close to degeneracy is also motivated by the possibility to use both signal and idler to pump the same ZGP OPO. This was first realized by Perrett *et al.* with a surface diffraction grating in an L-shaped cavity limiting the bandwidth of the double resonant type I OPO to 2 nm at degeneracy [67]. Phua *et al.* demonstrated the use of both the signal and the idler from a type II bulk KTP OPO by a wavelength dependent polarization rotator that aligned the polarization planes of both waves outside the cavity [13]. Since the signal and idler from the KTP OPO were separated by 60 nm the end result was, however, two separate OPOs in the same ZGP crystal.

3.3. ZGP OPOs

ZGP has high nonlinearity (d_{eff}=75 pm/V), which leads to a nonlinear figure of merit (d_{eff}^2 / n^3) about 9 times larger than for PPLN. The birefringence is suitable for type I phase-matching over a large range of wavelengths. For long wavelength generation type II phase matching is also possible. In addition ZGP has good thermal and mechanical properties, as well as an acceptable damage threshold (>1 J/cm^2). With improved polishing techniques the damage threshold can be raised to 2 J/cm^2 [69]. The transparency range is often reported as 0.74-12.4 μm, but low absorption is available only in the 2-8 μm region and a ZGP OPO thus needs to be pumped at wavelengths longer than 2 μm. The losses in the 1-4 μm region are dependent on defects and impurities in the crystal and the growth is thus very critical [70]. There have been a large number of ZGP OPOs reported in the literature; see for example references [8-14].

The acceptance bandwidth of a ZGP OPO is 6.5 nm×cm for pumping at 2.13 μm. The acceptance bandwidth is the limit where the pumping efficiency has decreased by a factor two for the power at the edges of the spectral pump profile. The pumping efficiency will thus increase further with narrower bandwidth. Perrett *et al.* reported a

decrease of slope efficiency from 33 % to 9 % when the pump bandwidth increased from 2.3 to 8 nm [67].

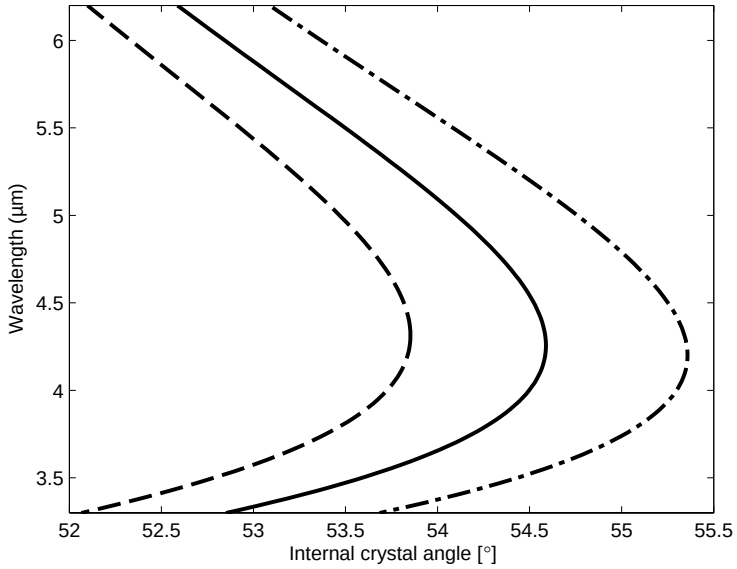

Figure 3-3. Phase matching curves for a ZGP OPO pumped by 2.1 (dash-dotted), 2.128 (solid) and 2.158 (dashed) μm. The 2.1 and 2.158 μm wavelengths could be a signal-idler pair from an OPO pumped by a 1.064 μm Nd^{3+}-laser.

In Figure 3-3 examples of theoretical tuning curves for pumping at three different wavelengths are shown. The two wavelengths 2.1 and 2.158 μm could be the signal and idler from a 1.064 μm pumped OPO. For the ZGP crystal angle that tunes the signal pumped OPO to degeneracy, the idler pumped ZGP OPO will already emit outside of the desired 3.5 to 5 μm wavelength band. It is thus evident that in order to phase-match an OPO simultaneously for the signal and idler from a 1 μm pumped OPO the first OPO has to operate very close to degeneracy while still maintaining narrow bandwidth. For a type I OPO this is possible only with the help of linewidth narrowing elements in the cavity.

3.4. OPO simulations

In many cases the understanding and optimization of an experiment is facilitated by a computer model. Analytical solutions of the coupled differential equations (2.12) that govern the OPO dynamics are only possible in very simplified cases. When including spectral bandwidth, dispersion, spatial modes, diffraction and thermal effects in the material the system becomes very complex. Numerical simulations are thus the only alternative. The Norwegian Defence Research Establishment, FFI, has provided the nonlinear optics simulation program Sisyfos for our use. This program was developed by Gunnar Arisholm at FFI and numerically solves the coupled differential equations governing the transfer of energy between different wavelengths with spatial and temporal resolution. The theoretical basis of Sisyfos is described in [71,72]. From the multiple electric field temporal sample points per roundtrip the optical spectra can be calculated. Sisyfos 4D that has been used in this work was implemented as a Matlab toolbox, which made batch processing of parameter variation possible.

A simulation of the near degenerate PPKTP OPO for varying separations between the nonlinear crystal and the VBG is included in paper V and the results are summarized in section 4.5.

Simulations were also performed on a generic plane wave ZGP OPO to study the dependence on the pump spectral characteristics. Results of these simulations were included in paper IV. The two main questions to be addressed by the simulations were:

- How does the OPO efficiency depend on the pump bandwidth at bandwidths smaller than the acceptance bandwidth?
- How will the output energy vary in a ZGP OPO that is pumped by two spectral lines with varying separation?

In the simulations a generic pump model with random amplitudes of the modes with a Lorentzian probability distribution and random phases was used. In the real case of one OPO pumping a second OPO the spectral properties are more complex. The effect of varying spectral bandwidth of a single pump beam is seen in Figure 3-4. The simulations show that the output power decreases with increasing pump bandwidth already at low bandwidths and that there is no threshold below which the efficiency is constant. The effect seems to be a combination of raised threshold and reduced slope efficiency.

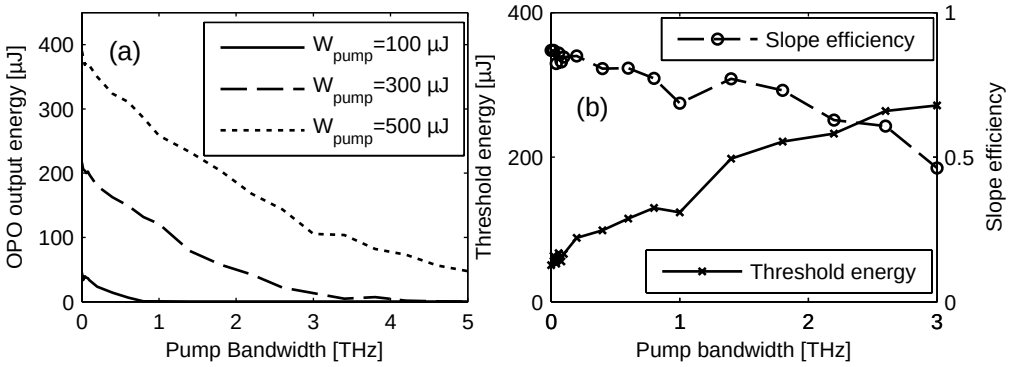

Figure 3-4. (a) Simulated ZGP OPO output energy as a function of pump bandwidth for three different pump energies. (b) Simulated OPO threshold energy and slope efficiency as a function of pump bandwidth.

The effect of pumping with a combination of two pump beams with different wavelengths is shown in Figure 3-5. From the comparison between applying the two pump beams separately and summing the output energy afterwards and applying both beams together in the same simulation it is evident that the conversion efficiency is enhanced by the coherent combination of the two pump beams. This enhancement of the conversion efficiency is strongest when the beams are degenerate in frequency, but is discernible all the way out to 1 THz detuning from degeneracy, corresponding to pumping with the output from an OPO tuned to 2113 and 2143 nm.

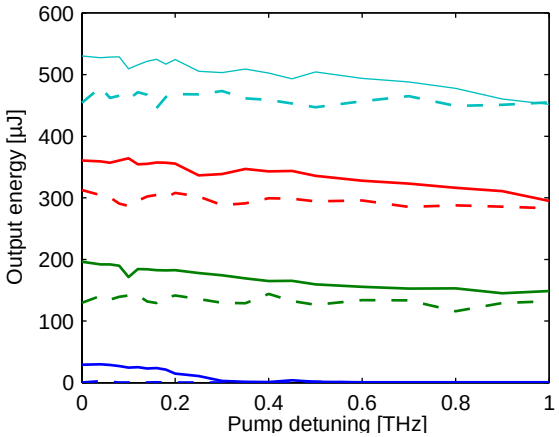

Figure 3-5. The calculated output energy of the ZGP OPO pumped by the signal and idler of an OPO with varying detuning from degeneracy. Solid lines are the simulations with both pump components applied simultaneously and dashed lines with the two components simulated separately and the generated energy summed afterwards. The total pump energies were 100, 300, 500 and 700 μJ with half of that energy in each component.

3.5. Volume Bragg gratings

Longitudinal diffraction gratings, called volume Bragg gratings, bulk Bragg gratings or volume holographic gratings, having a periodical modulation of the refractive index can be used to selectively reflect only one wavelength with the reflectance bandwidth orders of magnitude lower than what is possible with coated mirrors. This makes them an interesting alternative as cavity mirror for a narrow bandwidth OPO. A thorough review of the properties and applications of VBGs was given by Jacobsson [73].

Several different materials can be used to produce longitudinal gratings, but the most successful so far are photo-thermo-refractive (PTR) glasses. In the alumo-sodia-silicate glass materials that are doped with silver, cerium and flourine, illumination by ultraviolet light starts a photochemical process that after heat treatment results in a change of the refractive index [74]. By illuminating with a holographic technique or a phase mask a grating with period Λ according to $n = n_0 + n_1 \sin(2\pi x / \Lambda)$ can be created, as shown in Figure 3-6, where the modulation n_1 is up to 10^{-3} in magnitude.

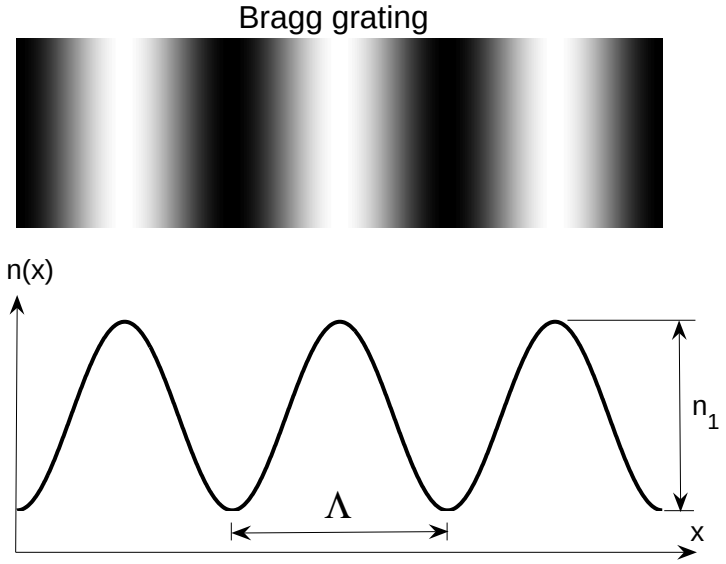

Figure 3-6. A volume Bragg grating has a sinusoidal index modulation in the propagation direction.

The glasses and the generated gratings are mechanically, chemically and thermally (to at least 400 ˚C) stable, show damage thresholds similar to normal mirror substrates and have low absorption in the visible and near IR (up to 2.7 μm). The reflected wavelength is determined by the Bragg condition

$$\lambda_B = 2n\Lambda\,. \tag{3.1}$$

The reflectance bandwidth is calculated according to

$$\frac{\Delta\lambda}{\lambda} = \frac{\lambda}{2nd} = \frac{\Lambda}{d} = \frac{1}{N}\,, \tag{3.2}$$

where d is the grating thickness and N is the number of grating periods in the material. The bandwidth can range from 0.01 nm to a few nanometres. This is many times narrower than the bandwidths achievable with multilayer coatings. The reflectance properties of thick hologram gratings were derived by Kogelnik [75]. Somewhat reformulated the amplitude reflectance at plane incidence can be expressed as

$$\rho = -\frac{\kappa \sinh\left(\sqrt{\kappa^2 - \delta^2}\, d\right)}{\delta \sinh\left(\sqrt{\kappa^2 - \delta^2}\, d\right) + i\sqrt{\kappa^2 - \delta^2}\, \cosh\left(\sqrt{\kappa^2 - \delta^2}\, d\right)} \tag{3.3}$$

with $\delta = 2\pi n_0 \left(\lambda^{-1} - \lambda_B^{-1}\right)$ and $\kappa = \pi n_1 / \lambda$. The peak diffraction efficiency is

$$R = \tanh^2\left(\frac{\pi n_1 d}{2 n_0 \Lambda}\right). \tag{3.4}$$

Maximum practical diffraction efficiencies are around 99 % for grating thicknesses larger than 10 mm. As n_1 and d are both adjustable parameters the bandwidth and the reflectivity can be varied independently.

The temperature dependence of the reflected wavelength is very weak. Some measured values are 23.4 pm/°C at 2479 nm [76] and 10 pm/°C at 1024 nm [77]. The wavelength change should be

$$\frac{\partial \lambda_B}{\partial T} = \lambda_B \left(\frac{1}{n}\frac{\partial n}{\partial T} + \alpha\right), \tag{3.5}$$

where α is the thermal expansion of the glass material. As the dispersion varies with the wavelength the wavelength change with temperature is not directly proportional to the Bragg wavelength, but the temperature sensitivity at 2.13 μm should be approximately 20 pm/°C. The temperature of the VBG is thus not an important parameter in designing the OPO for our applications.

Volume Bragg gratings are used in many applications and only some examples are given here. They can for example be used as optical filters [78], in spectral beam combination [79] and with longitudinal chirp as dispersive elements in ultrashort pulse compression [80]. One important application is their use as extracavity feedback elements for wavelength stabilization in diode lasers [81,82]. They have also been used as cavity mirrors in solid state lasers with Nd^{3+} [83], Er^{3+} [84] and Tm^{3+} [85] gain media, and in fiber lasers [86,64].

The first use of a VBG to limit the bandwidth of an OPO was reported by Jacobsson *et al.* in 2005 [15], where a 0.16 nm bandwidth 975 nm signal PPKTP OPO was demonstrated. After this demonstration other experiments have been presented in concurrence with the work described in this thesis. Tuneable OPOs have been achieved in different ways. In the first experiment tuning by a folded cavity design with variable angle of incidence was demonstrated [15]. This scheme was later improved using a ring cavity design with a VBG retroreflector [87]. Transversely chirped VBGs that are translated across the beam have shown larger tuning ranges [88], and a MOPA setup using this type of OPO as master oscillator has generated a tuneable UV source [77]. The IR range has been targeted with a high energy degenerate OPO at 2128 nm [89], and by a narrowband design using a cavity with two VBG [76]. Sum frequency mixing of a VBG OPO in the visible with a 266 nm beam has generated high quality deep UV light [90,91]. A very narrow bandwidth master oscillator using a VBG to limit the cavity feedback to a single transmission peak of an etalon has after amplification in an OPA been used as a pump source for a spectroscopic quality mid-IR DFG source [92]. Spectroscopic quality tuning of the idler from a CW OPO has been demonstrated by using a tuneable single frequency fibre laser as pump for an OPO where a VBG fixed the signal frequency [93].

4. Experimental results

4.1. Narrowband PPLN OPO

By using a volume Bragg grating as output coupler in the OPO the feedback in the cavity is limited to the desired wavelength. The output coupling is thus 100 % at all wavelengths that are not within the narrow reflection bandwidth of the VBG, and the threshold is never reached for broadband operation. At the resonance wavelength of the VBG the radiation is, on the other hand, reflected back with the diffraction efficiency R and the output coupling is thus 1-R. If the surfaces of the grating are properly antireflection (AR) coated the grating introduces no extra losses in the cavity compared to a standard mirror output coupler.

An experiment where the output coupler in a PPLN OPO was exchanged for a VBG resonant at 2008 nm was first reported in [A9] and [A12] and later in more detail in paper I. The setup is schematically shown in Figure 4-1. This showed that the results achieved by Jacobsson *et al.* shortly before [15], were transferable to the 2 μm range and to higher average powers. The narrowband VBG feedback limited the signal and idler spectra to narrow lines with bandwidths lower than the 0.5 nm resolution of the available grating monochromator. A comparison to the spectrum from the same OPO using a dichroic mirror output coupler is shown in Figure 4-2.

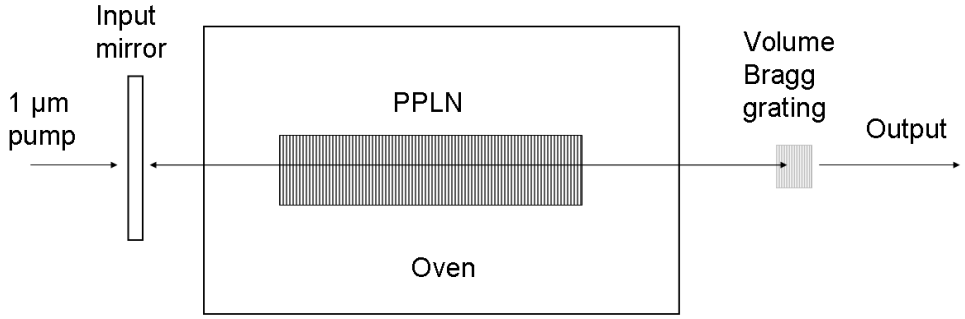

Figure 4-1. A schematic image of the PPLN OPO setup.

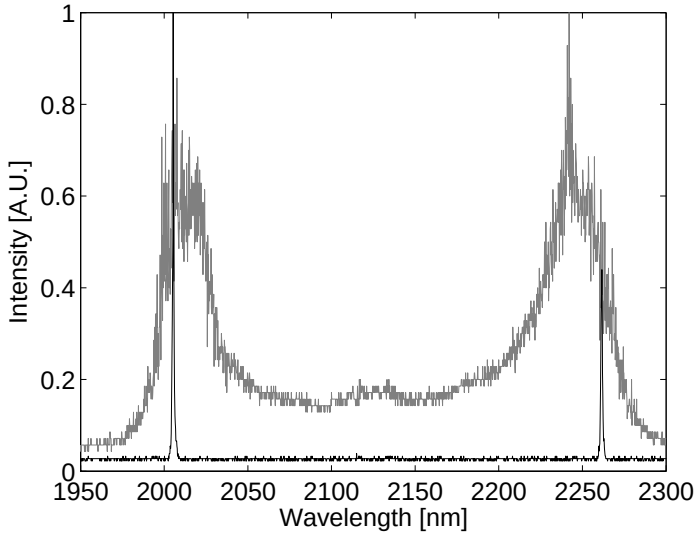

Figure 4-2. Spectrum of a PPLN OPO using volume Bragg grating [black] and a regular dielectric mirror [gray] output couplers.

The output pulse energy and depletion for the 10 kHz PRF OPO are shown in Figure 4-3. The OPO generate 1.6 W of average power in signal and idler with 4.4 W pump power, corresponding to 36 % device conversion efficiency. This figure is external efficiency not corrected for losses in the filter used to remove the non-depleted pump.

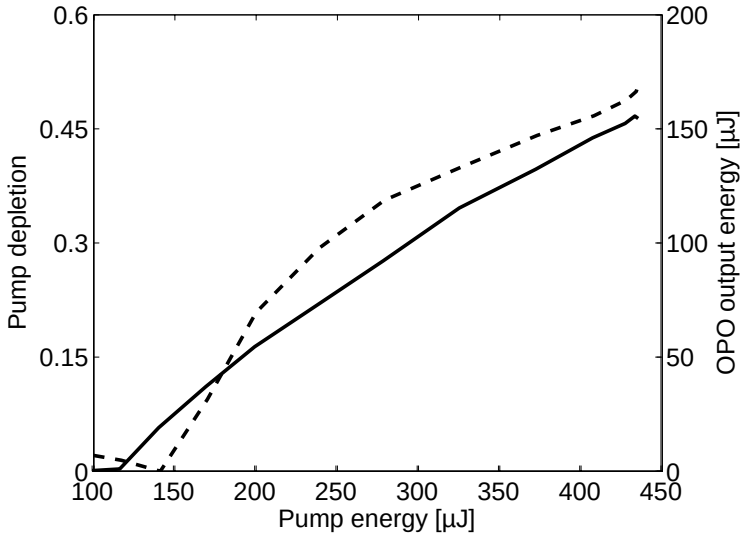

Figure 4-3. OPO output energy (solid) and single pass pump depletion (dashed)

4.2. ZGP OPO pumped by the signal of a narrowband PPKTP OPO

To provide higher energy for pumping of a second OPO with the signal from the OPO with the VBG an alternative setup was built using a flashlamp pumped Nd:YAG laser and a PPKTP crystal as described in paper II. A photograph of the OPO is shown in Figure 4-4. The spectral width achieved was similar to the PPLN OPO presented above and the maximum output energy was 1.4 mJ with 4.2 mJ pump energy.

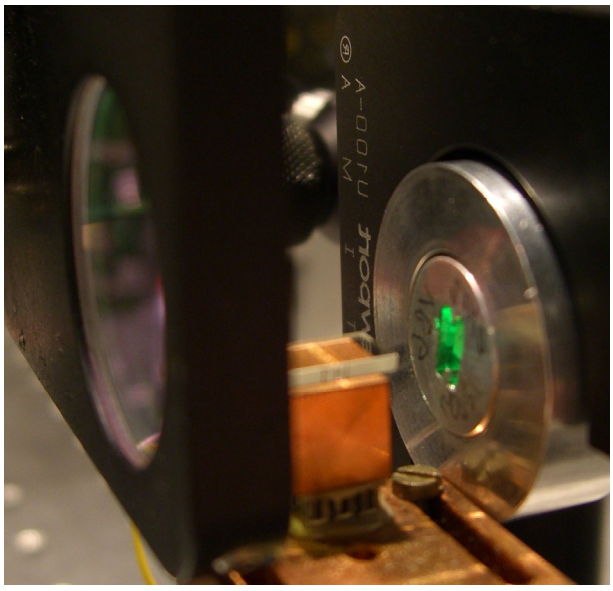

Figure 4-4. Photograph of the PPKTP OPO in paper II with the volume Bragg grating in the metal adapter to the right, the PPKTP crystal on the temperature controlled copper heat-sink in the middle and the incoupling mirror to the left.

The 2008 nm signal from the PPKTP OPO with a VBG output coupler was used to pump a ZGP OPO. The OPO cavity that consisted of two flat dielectric mirrors was doubly resonant and used double pass pumping. The 14 mm long ZGP crystal was angle tuned to provide gain in the mid-IR. The ZGP OPO had a slope efficiency of 41 % and a threshold of 38 μJ. The maximum output energy was 170 μJ using 400 μJ pump energy at 2008 nm and 4.2 mJ at 1064 nm. The mid-IR output energy and the corresponding pump depletion is shown in Figure 4-5. The idler at 2264 nm was discarded as the available ZGP crystal had a coating and a cut that was not suitable for pumping with this wavelength. The achieved conversion efficiency from 1 μm to the mid-IR was thus only 4 %, partly due to low transmission in the filters used to remove the remaining 1 μm pump and the 2.26 μm idler between the two OPOs.

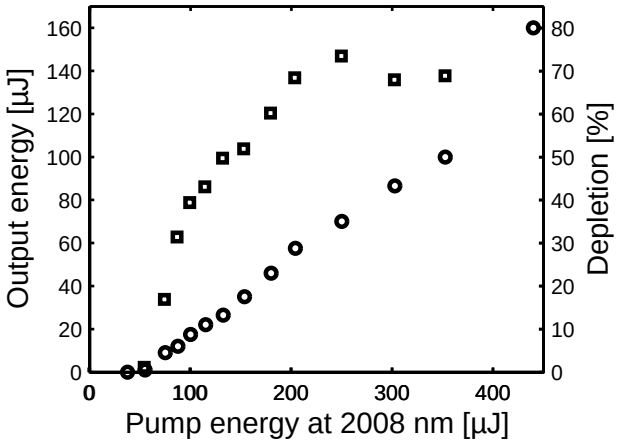

Figure 4-5. Output energy and depletion of the ZGP OPO pumped at 2008 nm that was described in II. The circles signify efficiency values and the squares depletion values.

4.3. ZGP OPOs pumped by near degenerate narrowband PPKTP OPOs

To increase the system efficiency it is desirable to use both the signal and the idler from the first OPO to simultaneously pump the ZGP OPO. This demands that the first OPO must operate much closer to degeneracy than in [II], as seen from Figure 3-3. We thus utilized a new set of volume Bragg gratings resonant around degeneracy at 2.13 μm. This setup, see Figure 4-6, that operated at 10 Hz PRF and produced up to 700 μJ at 2.13 μm in a double pass pump configuration was reported in paper III.

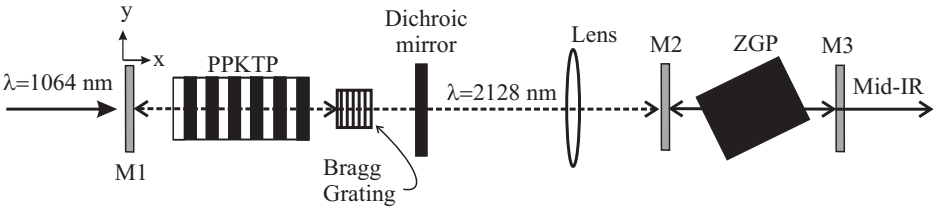

Figure 4-6. The experimental setup of paper III.

The output spectrum that is shown in Figure 4-7 contained two narrow lines separated by 0.6 nm and the full spectrum was contained in a 2 nm wide region around degeneracy. The setup was used both with the dichroic mirror aligned to back-reflect the pump in a double pass pump configuration and misaligned to dump the single pass depleted pump. As seen in Figure 4-8 double pass pumping as expected increased the output energy from the PPKTP OPO. The efficiency increase was however obtained at the cost of a slightly worse beam quality and therefore slightly

higher threshold for the ZGP OPO. The highest mid-IR output energy of 250 µJ at 7 % conversion energy from the 1.06 µm pump was still reached in the double pass pump configuration.

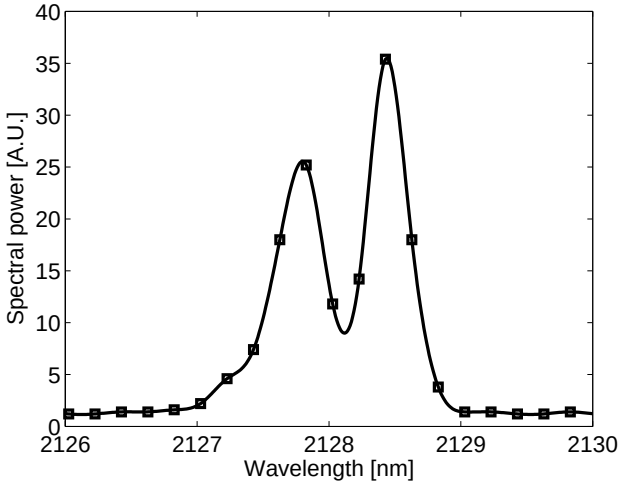

Figure 4-7. Spectrum of the output from the PPKTP OPO. Squares are measured values and the solid line is a spline interpolation.

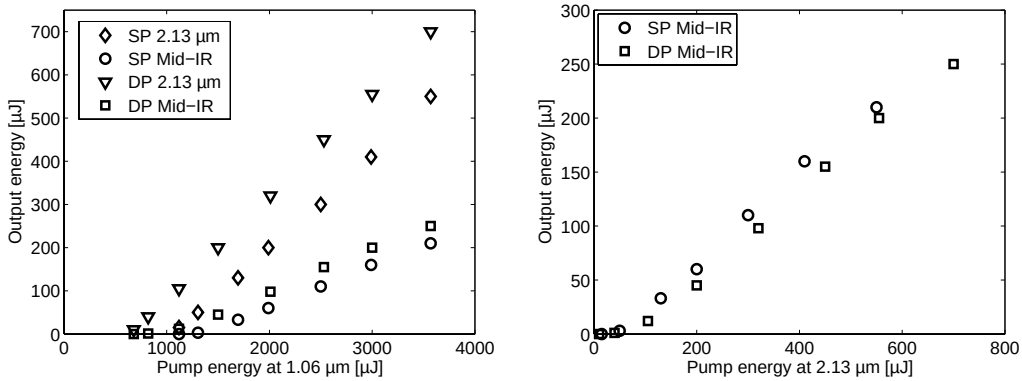

Figure 4-8. Output energy as a function of 1.06 µm (left) and 2.13 µm (right) pump energy. SP denotes single pass pumping and DP double pass pumping of the PPKTP OPO.

By turning the ZGP crystal and thus tuning the phase-matching conditions the output spectrum could be tuned from degeneracy to a signal wavelength of 2.9 µm. The corresponding maximum idler wavelength should be 8 µm, but the measurement was limited to 5.5 µm by the spectrometer sensitivity. The spectra in Figure 4-9 show that as expected from equation 2.24 the bandwidth of the type I OPO is very wide at degeneracy and then is reduced as the OPO is tuned away from degeneracy.

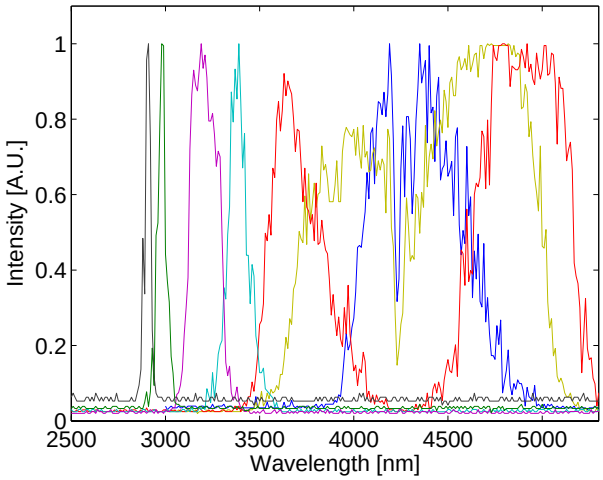

Figure 4-9. Spectra showing tuning of the ZGP OPO. The measurement was limited to around 5 µm, but from the measured signal wavelengths idler wavelengths up to 8 µm are expected. The dips at 4.2-4.3 µm is a result of the strong atmospheric absorption at these wavelengths.

A second setup that used a diode pumped Nd:YVO_4-laser with 20 kHz PRF was used to generate higher average powers. Even though the laser was protected by an isolator a single pass pump configuration was used to avoid thermal problems from the back-reflected pump. Up to 8 W average power was generated a few nanometres from degeneracy, and somewhat lower power exactly at degeneracy, as seen in Figure 4-10. These results were reported in [A24]. A similar experiment focused at high pulse energy instead of high average power was reported by Saikawa et al. [89], where they reported 61 mJ output energy with 1.4 nm spectral width around degeneracy.

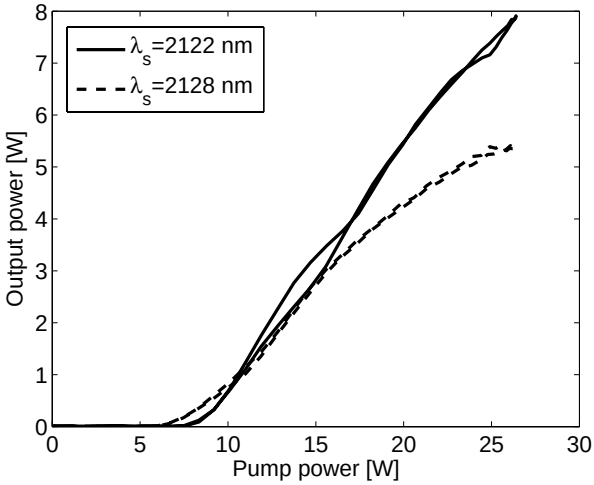

Figure 4-10. Output power as a function of pump power for two different VBG outcouplers, one very close to degeneracy (dashed line) and one 7 nm from degeneracy (solid line). The pump power was varied by rotating the half wave plate by 90° so that the pump power first increased and then decreased, hence the double lines.

The mid-IR output power from the ZGP OPO reached 3.2 W for a conversion efficiency of 12 % from 1.06 µm to the mid-IR. Because of the 13 nm difference of the PPKTP OPO signal and idler wavelengths pump tuning gives the ZGP OPO spectrum a double peaked nature, as shown in Figure 4-11.

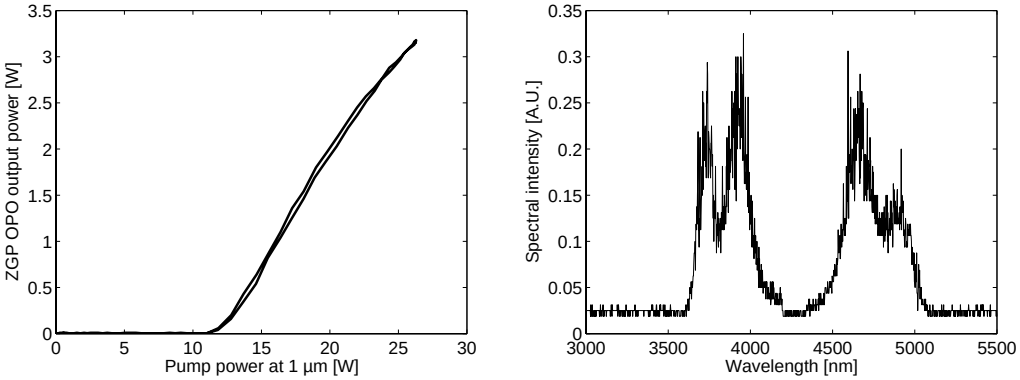

Figure 4-11. Output power and spectrum for the ZGP OPO pumped by the PPKTP OPO.

Since the signal and idler of the PPKTP OPO are so close to degeneracy the phase-mismatch for frequency doubling of the generated waves is very small. This introduces additional losses in the cavity by extra back conversion to wavelengths close to the pump wavelength. In addition difference frequency generation with the idler or signal introduces secondary wavelengths $\omega_{s2} = 2\omega_s - \omega_i$ and $\omega_{i2} = 2\omega_i - \omega_s$ in the OPO. This process can be viewed as four wave mixing (FWM) by cascaded $\chi^{(2)}$ interactions.

The generated wavelengths will be at a distance from degeneracy equal to three times the distance to degeneracy of the signal and idler. For the OPOs we study this is well within the gain bandwidth and the generated waves experience optical parametrical amplification. In a high gain system with a long crystal these secondary spectral peaks will reach macroscopic levels as seen in Figure 4-12, where the frequency doubled signal and idler also can be seen in the spectrum of the depleted pump. When measuring with higher sensitivity higher order FWM peaks caused by frequency doubling of the secondary peaks are detectable and they could also reach considerable amplitude if the single pass gain is high enough. As it is not certain that the secondary waves have the same divergence as the signal and idler we do not want to draw too strong conclusions on their magnitude from the measured spectra, but an estimate is that around 5 % of the energy is in the secondary peaks in our measurement. Similar FWM peaks have also been reported by Jacobsson *et al.* [88], where also Raman shifted signals were detected. Other parasitic loss mechanisms are evident from generation of low power visible light in the nonlinear crystal.

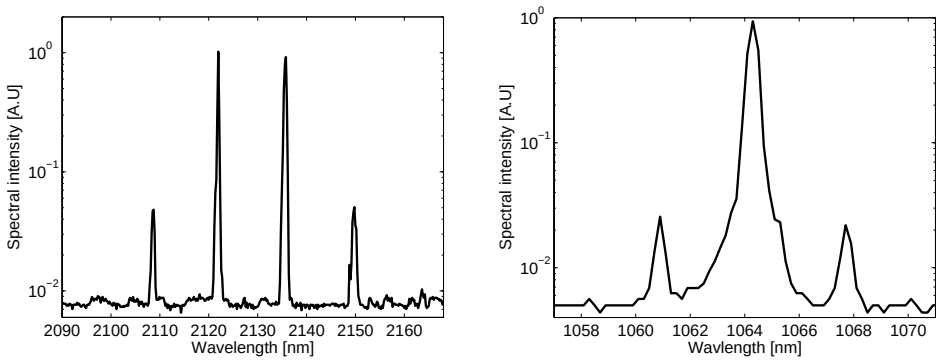

Figure 4-12. Left: Spectrum from the OPO showing the four-wave mixing peaks at 2109 and 2150 nm. Higher order FWM peaks are present at 2096 and 2164 nm even if hidden in noise in this figure. Right: Spectrum of the depleted pump with the frequency doubled signal and idler.

4.4. Spectral characterization of narrowband PPKTP OPOs

The OPO spectra reported in [I-III] were all measured using a grating monochromator with a resolution that was insufficient to determine the actual linewidth of the signal and idler generated in the OPOs using VBG bandwidth limiting. To gain better knowledge of the spectral properties of OPOs with VBG output couplers more thorough investigations were performed on one experimental setup. This setup used a commercial diode pumped Nd:YVO_4-slab laser (Edgewave IS4I-E), that for this experiment was run at 100 Hz PRF with a pulse energy slightly over 1 mJ. This is the same laser that was used for the high average power results in section 4.3. Characterization of the pump laser is reported in section 4.4.1. Theoretical calculations of mode separation are discussed in section 4.4.2 and compared to Fabry-Perot etalon measurements of the OPO spectrum in section 4.4.3. Experiments were performed with two PPKTP crystals of different lengths. The measurements, that resolved the longitudinal modes in the cavity, were performed using two different VBG, one very close to degeneracy and one a few nanometers off degeneracy.

4.4.1. Pump spectral characterization

The pump bandwidth was measured using an image flipping Michelson interferometer, see Figure 4-13. The laser beam was focused on the camera with a 4 m focal length lens to avoid effects from the multimode structure in the horizontal direction (M^2~2). The two beams interfering at an angle to each other on the camera will produce a set of vertical fringes. The visibility of these fringes was measured while the single mirror arm length was varied. In Figure 4-14 the visibility is shown normalized to the value at exactly balanced arm lengths. The maximum measured visibility was approximately 0.7, caused primarily by different intensities in the two beams. The FWHM width of the visibility peak can be determined to 4.5 mm, corresponding to 29 GHz spectral bandwidth for a Gaussian spectrum. The visibility is also shown for 123.9 mm translation. The good overlap of the peaks shows that the phase of the pump beam is periodic with a period time of 0.83 ns. We estimate that the diffraction effects on the visibility, because of different path lengths, are small and do not influence the measurement of the bandwidth [94].

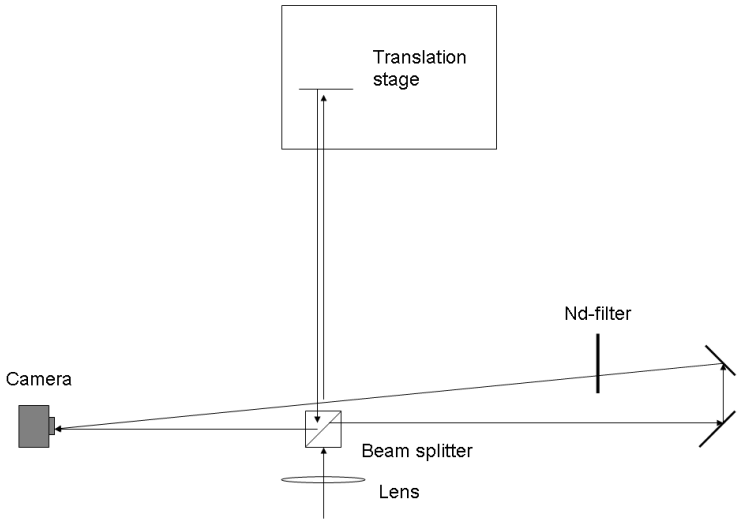

Figure 4-13. Image flipping Michelson interferometer used to measure the laser linewidth.

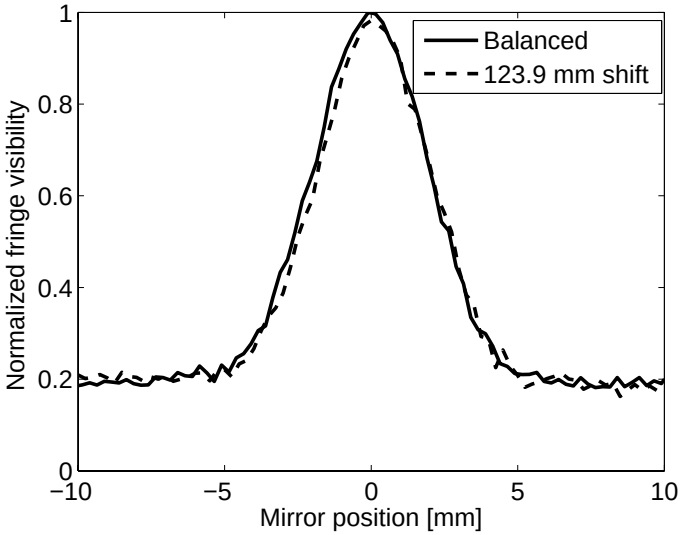

Figure 4-14. Normalized fringe visibility in an image rotating Michelson interferometer when translating one mirror.

If a photo-detector is placed in the laser beam the electric field of the laser beam will interfere with itself to create a homodyne beat-note spectrum. Assume that the electric field of the laser beam impinging on the detector can be separated in equidistant longitudinal modes according to

$$E(t) = \sum_j a_j(t) \exp\left[i2\pi(\nu_0 + jF)t + \varphi_j \right] + c.c., \tag{4.1}$$

where a_j and φ_j are the mode amplitudes and phases, F is the mode separation and ν_0 is the frequency of the mode with j=0. For laser modes $F \ll \nu_0$. The radio frequency (RF) components of the voltage U from the detector will then be

$$U(t) \propto I(t) \propto E(t)^2 = \sum_{j,k} a_j(t) a_k^*(t) \exp\left[i2\pi(j-k)F + i(\varphi_j - \varphi_k) \right] + c.c., \tag{4.2}$$

where I is the laser intensity and the indexes j and k cover all modes in the laser spectrum. In addition there will be high frequencies around $2\nu_0$ that can not be detected with the RF spectrum analyzer. The case of $|j-k|=1$ will produce the first beat note at $f=F$, $|j-k|=2$ the second at $f=2F$ and so on, where f is the frequency in the homodyne spectrum. For equal amplitudes, random phases and an infinite number of modes the interference signal would average to zero. The sum of finite amount of complex numbers will in general however not be zero, and averaging over a large number of laser pulses we get the beat-note spectrum. If the phases of the longitudinal modes are not random but related to each other, as in a mode-locked laser, the interference between different pairs of modes will sum coherently and the beat-note amplitude will be large.

The homodyne beat-note spectrum of our pump laser was recorded with an electrical spectrum analyzer and is shown in Figure 4-15. The 1.2 GHz separation of the peaks confirms the 124 mm optical linear path length in the laser cavity. The detection setup had approximately 12 GHz bandwidth and steady amplitude of the beat notes can be observed out to this frequency. The higher amplitude for the first two beat notes shows that there is some degree of correlation between neighbouring longitudinal modes in the pump laser. This correlation between neighbouring modes is a complex phenomenon that we so far have found no appropriate mathematical

model for. Gain induced mode locking in acousto-optically Q-switched Nd:YVO_4-lasers has been reported [95], and the mode correlations could be a similar phenomenon.

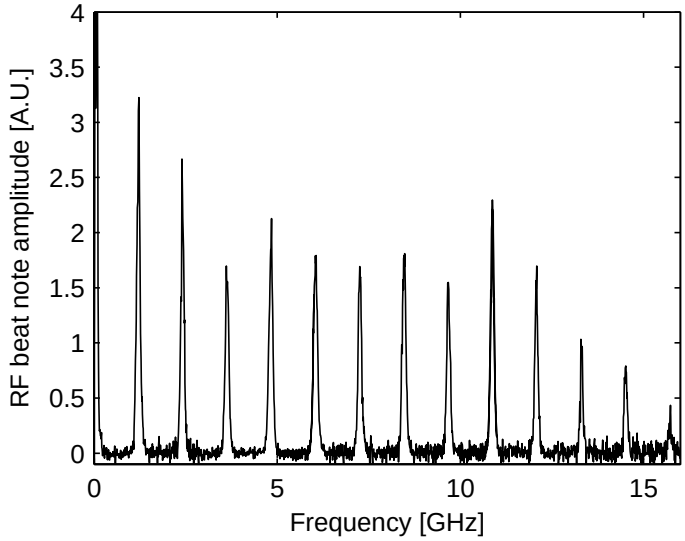

Figure 4-15. Homodyne laser interference spectrum.

4.4.2. Theoretical mode separation in a VBG cavity

Longitudinal modes in a cavity appear because of the demand that the optical field repeats itself after one roundtrip in the cavity. Thus the cavity roundtrip length must be an integer number of wavelengths. As the cavity length is constant this means that only discrete wavelengths can be resonant in the cavity. These frequencies are called longitudinal modes. Broadband laser radiation will thus not have a continuous spectrum, but the laser spectrum consists of discrete spectral lines under an envelope that defines the laser linewidth. In an empty two mirror Fabry-Perot cavity the modes are separated in frequency by

$$\Delta\nu = \frac{c}{2L}, \tag{4.3}$$

where L is the separation of the two mirrors. In the general case the mode separation can be expressed as

$$\Delta\nu(\lambda) = \frac{1}{\tau(\lambda)}, \tag{4.4}$$

where $\tau(\lambda)$ is the wavelength dependent roundtrip time in the cavity.

If one of the cavity reflectors is a VBG the group delay caused by varying penetration depths in the VBG will cause the mode separation to vary with wavelength. Dispersion in any materials inside the cavity will also cause weak wavelength dependence, but this effect can usually be neglected over the reflectivity bandwidth of a VBG. The total roundtrip time in the cavity can be expressed as

$$T_{RT}(\omega) = \frac{2}{c}\left(n_c(\omega)L_c + L_{air}\right) + d\phi/d\omega_{VBG}\big|_{\omega} \tag{4.5}$$

where n_c is the refractive index of the nonlinear crystal, and L_c and L_{air} are the physical lengths of the crystal and the air gaps in the cavity. The phase of the radiation reflected by the VBG can from eq. 3.3 be expressed as

$$\phi = -\arctan\left(\frac{\delta}{\sqrt{\kappa^2-\delta^2}}\tanh\left(\sqrt{\kappa^2-\delta^2}\,d\right)\right)+m\pi+\alpha, \tag{4.6}$$

where m is an integer defined to make the phase continuous and α is an arbitrary constant to give the right total phase shift compared to a chosen reference plane.

In a cavity with a 10 mm long PPKTP crystal, 3 mm air and with a VBG having 50 % reflectivity and 0.4 nm bandwidth (FWHM) the mode separation at the reflectance peak is 6.39 GHz as seen in Figure 4-16. At the first zero in the reflectivity function, 0.38 nm away from the peak reflectivity the mode separation has decreased to 6.15 GHz, a change of 4 %. As the diffraction efficiency is close to zero for the lowest mode separations there will be no oscillating modes here and the actual variation of the mode separation will be smaller than the theoretical maximum. The 0.4 nm bandwidth is only 27 GHz which means that only a few modes will oscillate.

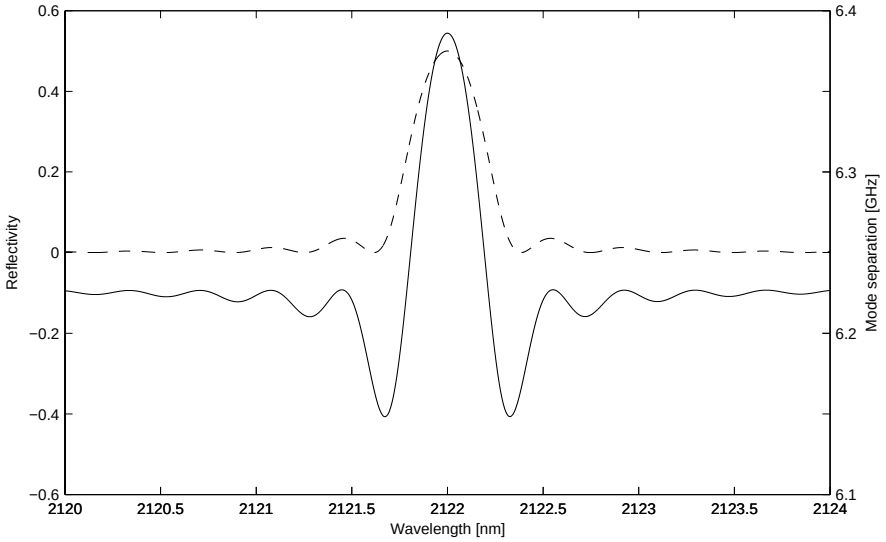

Figure 4-16. Reflectivity of a VBG (dashed line) and mode separation (solid line) of a cavity with a 10 mm long PPKTP crystal, 3 mm air and a VBG as one end reflector.

4.4.3. Fabry-Perot etalon measurements of OPO spectrum

Detailed studies of the spectrum were undertaken for PPKTP OPOs pumped by a diode pumped Nd:YVO_4-laser and reported in paper IV. To avoid thermal effects in the OPO the laser was run at 100 Hz PRF. For the measurements two different volume Bragg gratings were used, one resonant at 2122 nm and one resonant very close to degeneracy at 2128.6 nm. Low resolution grating monochromator spectra and as a comparison the spectrum of an OPO with a mirror output coupler are shown in Figure 4-17. In addition to the two VBG also two different PPKTP crystals were used, one with 10 and the other with 20 mm physical length.

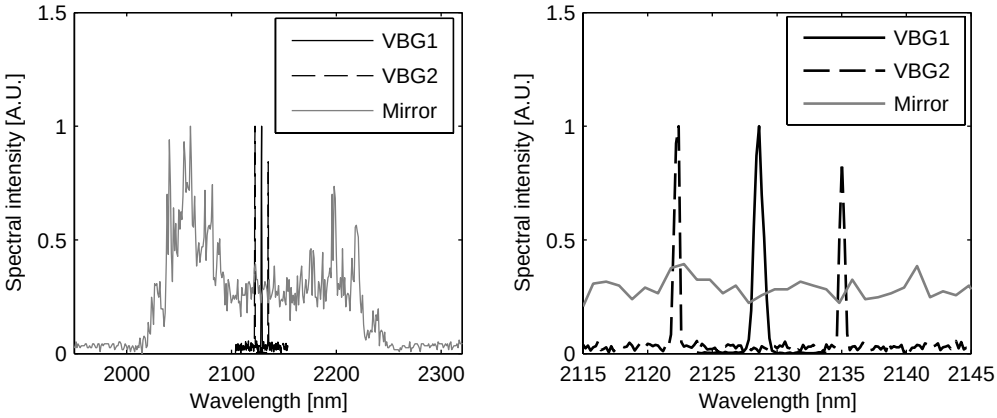

Figure 4-17. Output spectra from the OPO using three different output couplers shown at two different wavelength scales.

To obtain higher resolution in the spectral measurements a scanning Fabry-Perot etalon was used. This etalon uses two high reflectivity mirrors with adjustable separation to create a Fabry-Perot cavity with a finesse reaching approximately 70. The separation of the signal and idler with the 2122 nm VBG was larger than the free spectral range, but the etalon was adjusted so that different orders of signal and idler transmitted through the Fabry-Perot etalon were interleaved without overlapping of the individual peaks. One of the mirrors was then scanned a distance of a few wavelengths during 500 s and the transmitted energy recorded versus time for each laser pulse. From the knowledge of the free spectral range and the period time in the measurement the spectral width of signal and idler can then be calculated. These local spectra for signal and idler for the shortest possible OPO cavities with a 20 mm and a 10 mm long PPKTP crystal are shown in Figure 4-18 and Figure 4-19, respectively. The FWHM spectral widths are estimated as 10 GHz for the signal and 20 GHz for the idler, respectively. The longitudinal modes of the signal can in both cases be readily seen, and the mode separation is consistent with equations 4.2-4.4. The resolution is not good enough to see any variation of the distance between modes caused by the group delay dispersion.

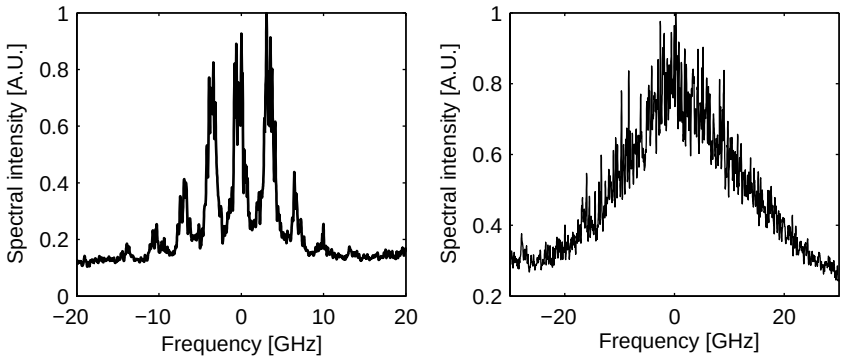

Figure 4-18. Spectra of signal (left) and idler (right) separated by 13 nm (900 GHz) measured by Fabry-Perot etalon at maximum pump power for the longer cavity (20 mm PPKTP crystal)

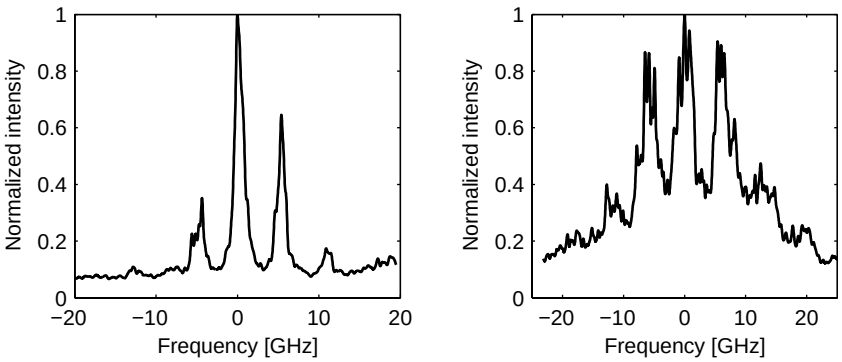

Figure 4-19. The signal (left) and idler (right) spectra of the short cavity OPO (10 mm PPKTP crystal) measured by the Fabry-Perot etalon. The signal and idler are separated by 13 nm (900 GHz).

In the longer cavity several longitudinal modes have almost the same amplitude while in the shorter cavity the mode separation is so large compared to the VBG bandwidth that one mode dominates. In [A19] a measurement close to threshold where almost all energy is in a single longitudinal mode is presented. An OPO using VBGs for both cavity mirrors where the FWHM of the signal spectrum is less than the mode separation has been reported [76], but unfortunately they did not present measurements that prove that there was only one mode oscillating.

The idler spectrum shows clear modulations at the mode separation of the signal for the shorter cavity (Figure 4-19), something that is not evident for the longer cavity (Figure 4-18). The peaks are attributed to correlation between modes in the pump and signal over a limited spectral width. The spectral peaks are wider than the measurement resolution, and are thus represented at approximately their actual width. This width should correspond to the maximum correlation distance, which can also be seen in the homodyne spectrum of the pump (Figure 4-15). As this width is larger than the mode separation in the longer cavity no modulation of the idler can be seen here.

Operating almost exactly at degeneracy we can see how there are no longer separate signal and idler peaks in the spectra of Figure 4-20. It is however still evident that there are longitudinal modes mainly on one side of degeneracy. Total bandwidths are estimated to less than 40 GHz FWHM.

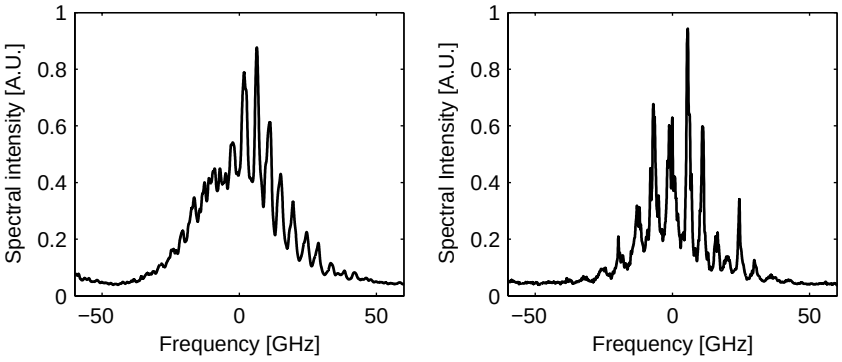

Figure 4-20. Spectra measured by a Fabry-Perot etalon of two OPOs using the same VBG resonant very close to degeneracy, but with different crystal lengths. Left: the long cavity OPO with the 20 mm PPKTP crystal. Right: the short cavity OPO with the 10 mm PPKTP crystal.

4.5. Length matching resonances in singly resonant OPOs

The fact that a laser beam is produced by oscillations in a cavity does not only make the spectrum of a multi-longitudinal mode laser consist of discrete spectral lines with a frequency separation according to equation 4.4, but also causes the pump beam for the OPO to be periodic with the roundtrip time in the laser cavity. The instantaneous power is determined by the coherent addition of the electric field of the different longitudinal modes. Addition of a number of waves with different frequency and phase will in general cause a rapidly varying interference pattern. In the Q-switched laser case the phases are random but constant and the output consists of a pulse that is several roundtrips long, but where there is a pattern of spikes under the pulse envelope that repeat itself with the roundtrip time. A more extreme case of interference of longitudinal modes is the mode-locked laser that emits an ultrashort pulse every cavity roundtrip because the different modes interfere constructively only once per roundtrip and cancel each other at all other times.

It was theoretically postulated in 1966 by Harris that the threshold of a doubly resonant OPO pumped by a multimode laser would be reduced by the coherent amplification of a single signal mode by the DFG of the pump and idler modes if the mode separations of pump laser and OPO matched [96]. Shortly thereafter it was also experimentally proven [97]. Much later the equivalent phenomenon of increased output energy from a doubly resonant OPO when the roundtrip times of the OPO and the laser matched was rediscovered by Arisholm *et al.* [18]. In this case the effect was explained in the time-domain by the fact that the instantaneous phase of the pump would repeat every roundtrip. As the signal and idler waves also have the same periodicity the phase combination that gives optimum gain and started the oscillation will be present also in later roundtrips, thus maximizing the conversion efficiency. In this work also the case of fractional cavity length ratios where e.g. every third laser mode coincides with an OPO mode was discussed. For the singly resonant case neither of these fundamentally equivalent explanations holds as the idler wave is free to adapt its phase in a new way on every roundtrip and the idler spectrum is not limited to cavity modes. Simulations of a broadband SRO pumped by a multi-longitudinal mode beam [98] have revealed weak cavity length resonances present only close to the threshold, except when a pump beam with very strong amplitude modulations was used. In that case the length resonances were stronger and persisted higher above threshold.

In measurements of a DRO with a dielectric mirror output coupler clear resonances of the output power at certain OPO cavity lengths were found, see Figure 4-21 [V]. This is the same effect earlier reported by Arisholm *et al.* [18].

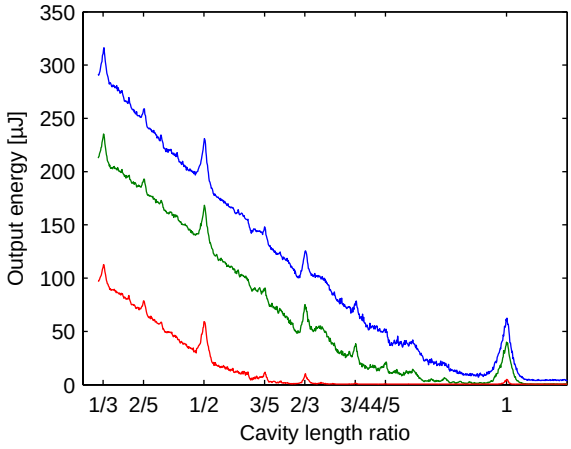

Figure 4-21. Average OPO pulse energy as a function of cavity length ratio from a DRO with mirror output coupler. The pump pulse energies were 0.99, 0.93 and 0.73 mJ.

By using a VBG resonant at 2122 nm we have an output coupler with extremely low feedback at the idler wavelength. The VBG was fabricated with the grating planes at an angle to the surface and the PPKTP crystal was polished with a slight wedge. There are thus no surfaces with the normal parallel to the propagation direction, except the input coupling mirror. The OPO will in this way be perfectly singly resonant with no idler feedback from parasitic reflections.

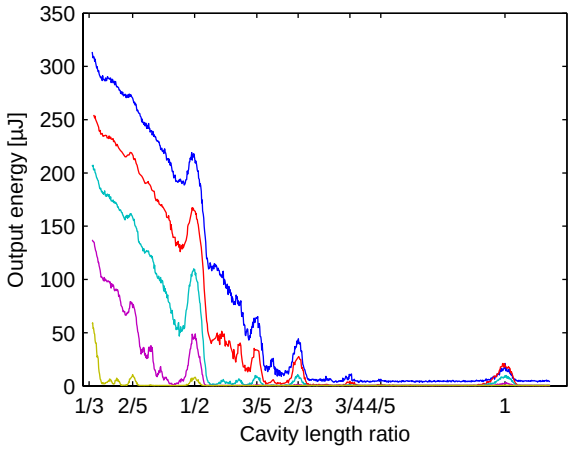

Figure 4-22. Average OPO pulse energy as a function of cavity length ratio from a SRO with VBG output coupler. The pump energies were 0.99, 0.93, 0.82, 0.67 and 0.50 mJ.

We report an experimental demonstration of cavity length resonances in a multi-longitudinal mode pumped SRO in paper V. In Figure 4-22 the variation of the output energy with cavity length ratio for the SRO using the VBG is shown. Resonance peaks are clearly seen on the decreasing slope. It is evident that in contradiction to for the DRO the amplitude of the peaks is decreasing with increasing output energy for the SRO. To further illustrate the differences between the DRO and the SRO the peaks around cavity length ratio ½ are shown in Figure 4-23 with a baseline subtracted. The baseline was constructed by fitting a third order polynomial to the points that are not close to any resonance. In Figure 4-23 it is evident that the SRO peak is wider and is surrounded by dips in output energy that are not present for the DRO. Comparing the peaks at 2/5 and 3/5 it is also evident that these have the same

amplitude for the DRO, while for the SRO the 3/5 peak where the OPO operates closer to threshold is much higher than the 2/5 peak.

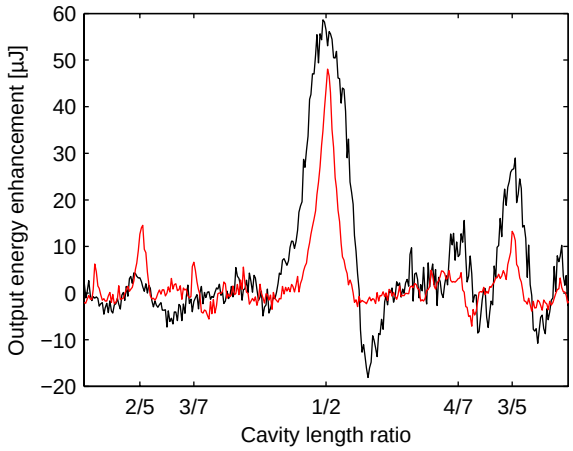

Figure 4-23. Enhancement peak with general slope subtracted at cavity length of OPO around ½ of laser cavity length. The black curve is with the VBG and the red curve is with the mirror output coupler, in both cases with 0.99 mJ pump energy.

In order to study additional aspects of the SRO length resonances a plane wave simulation model was set up in Sisyfos [71,72]. Because of the plane wave approximation that was needed to keep the computer run time reasonable the model neglected diffraction losses and the general slope as a function of cavity length was thus weaker than in the experiment. Otherwise the qualitative agreement with the experiments was good. The decline of the peak amplitude with increasing output energy and the dips around the peak for cavity length ratio 1 are evident in Figure 4-24.

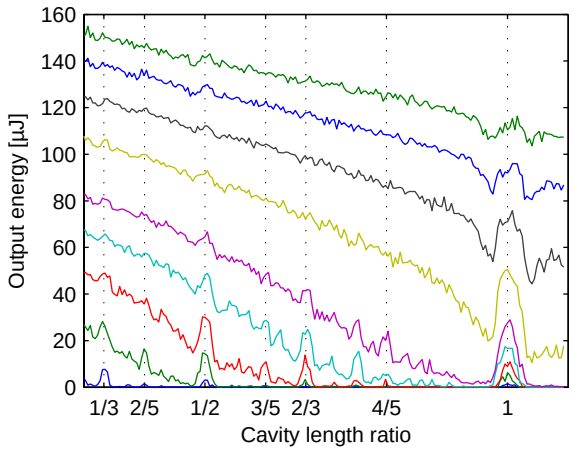

Figure 4-24. Simulated output energy from OPO in plane wave simulation. The pump energies are from the bottom 100, 125, 150, 175, 200, 250, 300, 350 and 400 µJ.

The origin of the resonance peaks in the SRO is the periodic spike pattern in the pump pulse. As the gain is proportional to the instantaneous pump power the signal intensity will grow faster at the pump intensity spikes. If on the next cavity roundtrip the generated signal again propagates together with the spike one period later in the pump the gain will again be higher and the OPO reach threshold faster for this part of the roundtrip period. This is illustrated in Figure 4-25 that shows the pump and the generated signal from a simulation with cavity length ratio 1. The selected time period can from the left pane be seen to have decreasing roundtrip averaged pump power

while the signal power is still increasing, as evidenced by more "micro-pulses" appearing at times in the roundtrip that correspond to lower amplitude pump spikes. Correlation between the longitudinal modes in the pump laser will increase the contrast of the spikes and thus increase the strength of the cavity length resonances. The limiting case is synchronous pumping with mode locked lasers, where the necessity of length matching is a well known fact [99,100].

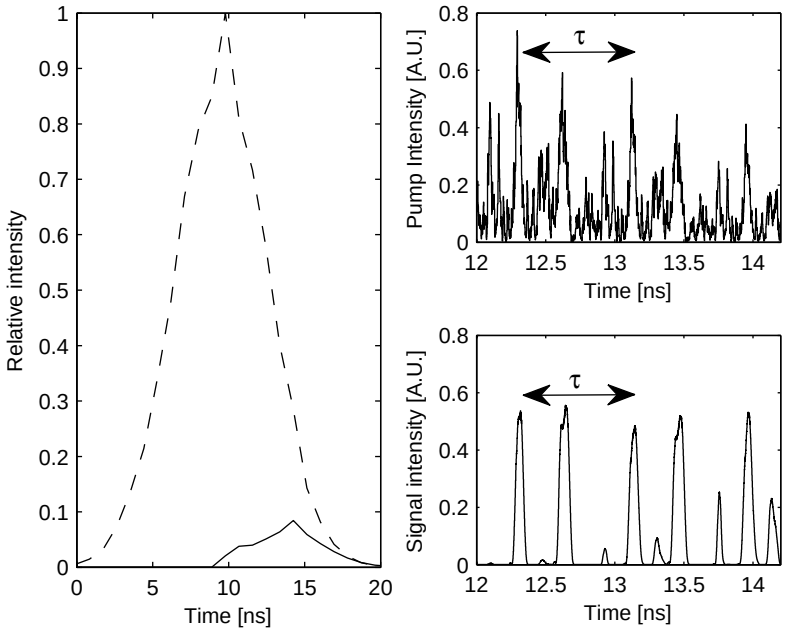

Figure 4-25. Results of a simulation with equal mode separations for pump laser and OPO showing the power after the input coupler. The simulation was done with 6 GHz pump bandwidth to make pump intensity variations slower. (Left) Roundtrip averaged pump (dashed) and signal (solid) intensities. (Upper right) Instantaneous pump intensity. (Lower right) Instantaneous signal intensity. τ denotes the periodicity due to the cavity roundtrips.

The presence of the dips surrounding the length resonances in a SRO is a clear indication that the SRO resonances are in fact the result of time-periodic coherent addition to the signal field for consecutive passes in the SRO cavity. Considering that the pump and the SRO signal mode spectra are fixed by the respective cavities, a small change in the SRO cavity length will result in the situation where a number of pump Fabry-Perot modes will correspond to the minima of the signal Fabry-Perot modes, i.e. these pump modes will for the consecutive passes interact with the signal field phase-shifted by $\pi/2$. This will result in periodic and coherent deamplification of the parts of the signal field, producing dips in the output energy. This effect is not observed in DRO, as seen in Figure 4-21, because the signal and idler spectra in DRO will change in response to the cavity length variation, for instance by starting to oscillate on other mode clusters where the gain is stronger.

5. Directed infrared countermeasures and beam propagation

The laser source development reported in this thesis was motivated by the need of better mid-infrared laser sources for directed infrared countermeasures (DIRCM). Here I give a simplified description of the manner in which DIRCM systems work. In addition I describe investigations I have performed on beam propagation in severe optical turbulence, such as may be experienced by aircraft mounted DIRCM system.

5.1. DIRCM principle

Missiles with infrared seekers are one of the largest threats against military aircraft. Because of the proliferation of small man-portable air-defence systems (MANPADs) they are a serious problem in asymmetric conflicts, such as peace keeping operations. There have been a large number of attacks causing a significant death toll by guerrilla forces around the world and attacks against civilian aircraft have also occurred [1]. To protect the aircraft the development of countermeasures against infrared seekers has been ongoing for almost as long as the development of the seekers themselves.

Aircraft self-protection systems are often called defensive aids suites (DAS). A DAS for protection against IR-guided missiles generally consists of a missile approach warning system (MAWS), a control system and a countermeasure system. Early countermeasures included infrared flares that emitted a stronger signature than the aircraft and made the seeker follow the flare when it detached from the aircraft. Other efforts used modulated flashing lamps on the aircraft [101]. Now the lamp based systems have been replaced by laser systems for directed infrared countermeasures (DIRCM). A DIRCM system generally uses an IR camera to track the direction to the missile that was detected by the MAWS. This tracking signal is used to direct the modulated DIRCM laser beam towards the missile to jam the missile seeker. The short discussion here about seekers and jamming of seekers with DIRCM systems is based on [102].

All objects emit black-body radiation with a temperature dependent power and wavelength distribution. An aircraft will give a bright contrast against the cold sky background, especially from the hot metal by the engine exhaust and from the emission of the hot exhaust gasses themselves. This radiation, with a peak wavelength in the mid-IR, can be used to lock on a target by IR-guided missiles. Non-imaging IR seekers produce a modulation of the collected target infrared signature by using rotating elements in the optics path. The seeker electronics then translates this modulated detector signal to a direction inside the field of view of the seeker. By adding a modulated laser beam to the passive target signature it is possible to make the seeker believe that the target is in another direction. A simple schematic example of jamming of a spin-scan seeker is given in Figure 5-1. Depending on the specific modulation of the jamming laser this may cause the missile to turn until the target is lost from the field of view of the seeker, e.g. optical break-lock, starting to wobble so that the flight gets unsteady and the missile is destroyed by aerodynamic forces or simply to miss the intended target.

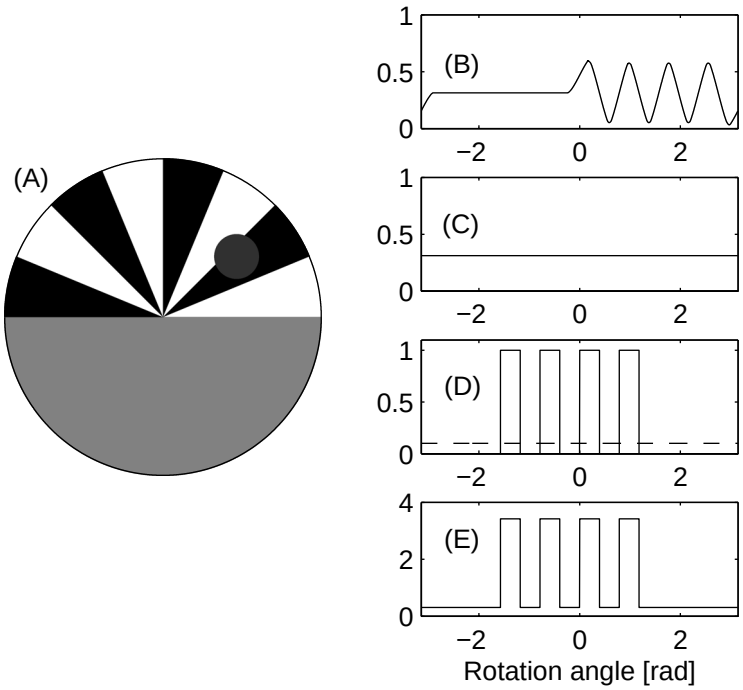

Figure 5-1. A: The spin-scan seeker works by rotating a reticle plate placed in a focus in front of the detector. The reticle has transparent, semi-transparent and opaque areas. A blurred spot of a point target is shown as a grey area off-axis. B: The modulated detector signal generated by the target spot in (A). C: If the target is centred on the seeker the target signal will be constant. D: A simple jamming signal modulated in time is added by the DIRCM system (solid) to the target signature (dashed). E: The power incident on the detector from an on axis target emitting a modulated laser beam will induce a modulation as if there was an off-axis target present. The seeker will then give rudder signals to the missile and may make it loose the tracking of the target (Optical break-lock). The jamming example given here is very simplified and may not be effective against actual seekers.

Modern imaging seekers use a focal plane array sensor to view the scene and different image processing algorithms to determine the direction to the target. They often include sophisticated methods to discriminate against simple countermeasures, such as hot flares that are ejected from the target. Jamming techniques using laser systems include saturation of the detector array and modulation of the laser power to cause the automatic gain control (AGC) of the sensor to oscillate the gain and thus prevent the seeker from tracking the target present in the image.

The development of laser sources for DIRCM evaluation systems has been the main topic of the work presented in this thesis. The laser sources that were developed are being used for different experiments to determine the effectiveness and limitations of laser based deception and jamming of missile seekers.

5.2. Laser beam propagation in severe turbulence

One important factor for the DIRCM system to be effective is that the laser power emitted has to be collected by the seeker's detector aperture. Getting enough power on the aperture involves not only producing high beam quality laser radiation in the seeker wavelength range, but also to transmit the beam in the right direction even though the aircraft is vibrating and both the aircraft and the missile are moving at high velocities. Even if tracking and pointing systems are working perfectly the modulation

waveform received by the seeker may still not be equal to what is transmitted because of turbulence distortion in the air.

Turbulent motion of the air causes variation of pressure and temperature of the air which in turn leads to randomly varying refractive index, called optical turbulence. The refractive index can be described by the Lorentz-Lorenz equation

$$\frac{n^2-1}{n^2+2} = \sum R_i \rho_i \,, \tag{5.1}$$

where ρ_i is the partial density of gas species i and R_i is the wavelength dependent refractivity constant for that gas species. The gas density can be coupled to temperature and pressure through the ideal gas law. When n is close to 1, which is valid for gases, (5.1) can be simplified to the Gladstone-Dale equation

$$n-1 = \sum k_i \rho_i \,, \tag{5.2}$$

where k_i is the Gladstone-Dale constant and $R_i = 0.625 k_i$. Gladstone-Dale constants are almost constant for wavelengths beyond 0.5 μm, so that even though values given in the literature are often for the visual range this only introduces a small error [103].

The strength of the turbulence is often characterized by the refractive index structure constant C_n^2, which is defined from the structure function. The structure function is in turn defined as

$$D_n(\vec{r}) = \left\langle \left(n(\vec{r_1}) - n(\vec{r_2}) \right)^2 \right\rangle, \tag{5.3}$$

where $\vec{r} = \vec{r_1} - \vec{r_2}$ and $\langle\ \rangle$ means ensemble average. The structure function can be defined in a medium that is locally homogenous and isotropic, which means that the mean refractive index varies slowly and there is local rotational symmetry.

In a statistically homogenous and isotropic medium Kolmogorov found that

$$D_n(r) = C_n^2 r^{2/3} \,,\ l_0 < r < L_0 \tag{5.4}$$

with $r = \left|\vec{r}\right|$ [104]. The inner (l_0) and outer (L_0) scale lengths are the scale sizes of the turbulent flow pattern, where turbulent vortexes smaller than the inner scale are lost to heat by the viscosity of the fluid. In the atmosphere typical values of the parameters in (5.4) are $C_n^2 = 10^{-15}$ to 10^{-13} $m^{-2/3}$, l_0 a few millimeters to a few centimeters and $L_0 = 10$ to 100 m depending on altitude above ground [105].

A simplified model of optical turbulence is that small volumes of higher or lower refractive index than the surrounding air work as lenses. If the “lenses” are larger than the laser beam they cause the beam to change direction. “Lenses” smaller than the laser beam size distort the beam so that it breaks up in several sub-beams. During its path the laser beam passes many “lenses” of different size. As the air is in constant motion the beam distortions vary over time. The motion of the center of gravity of the beam profile is called beam wander. For a detector smaller than the beam size the changing beamlets will cause a varying incident power. This phenomenon is called scintillation, and is also the cause of the apparent twinkling of stars [106].

The hot exhaust gases that are emitted from an aircraft engine at high speed will cause extremely high turbulence levels when the exhaust is mixed with the ambient atmosphere as there are high temperature gradients, varying chemical composition

and a turbulent flow. As a DIRCM system needs to protect the aircraft also from missile attacks coming from behind it is important to study the effects on a laser beam of propagation through the regions of high turbulence behind an engine exhaust. This has been done in the collaboration TA108.019 "Laser Beam Propagation and Imaging through severe Environments," between France, Germany, the Netherlands, Sweden and the United Kingdom.

Experiments to study the laser beam propagation in the exhaust plume from a jet-engine have been performed using a down-scaled jet-engine test-rig at Volvo Aero Corporation in Trollhättan [A25]. In the experiments a PPLN OPO based laser source developed by the candidate was used. The laser was placed so that the beam propagated past the engine and then parallel to the engine plume, as if it was placed on the fuselage or a wing and was pointed straight backwards. The laser beam thus propagated through the edges of the engine plume. Far behind the engine the laser beam was incident on an aluminium screen and the spot was imaged by infrared cameras. The laser used a PPLN OPO to simultaneously emit 1.5 and 3.6 µm beams. Examples of beam profiles recorded after propagation through the plume are shown in Figure 5-2. The aberrations causing beam break-up scale inversely with the wavelength, which is apparent from the larger distortion of the 1.5 µm than the 3.6 µm beam. The measured beam wander as a function of engine thrust and of distance from the engine axis is shown in Figure 5-3. The beam wander is nearly insensitive to wavelength, but clear trends with engine thrust and position are evident.

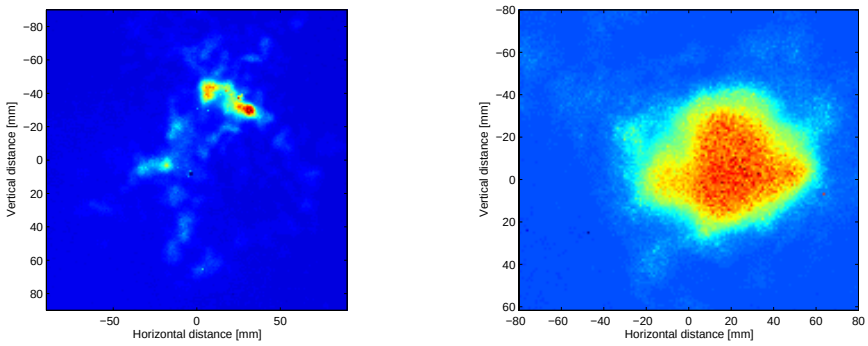

Figure 5-2. Examples of single laser pulses when the engine is running. To the left the 1.5 µm beam and to the right the 3.6 µm beam, respectively. The origin is defined as the average centroid position.

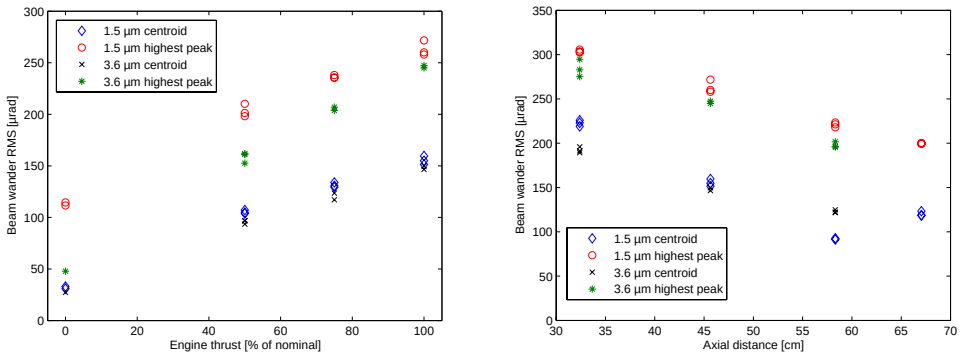

Figure 5-3. Root-mean-square (RMS) beam wander for laser beams propagating parallel to the engine axis. Left as a function of engine thrust and right as a function of the distance between the engine axis and the laser beam.

From an extrapolation of the formulas for beam wander from weak to strong turbulence it was determined that the beam had propagated through areas where C_n^2 was on the order of 10^{-9} $m^{-2/3}$ [A25]. This value is several orders of magnitude higher than in the free atmosphere. By comparing the C_n^2 values extracted from experimental data with the turbulence levels in the atmosphere it was found that the engine-related turbulence effects will dominate over the atmospheric turbulence effects for propagation distances up to several kilometers if the laser beam propagated through the exhaust plume.

6. Description of work and authour contribution

Paper I
Narrow linewidth 2 μm optical parametric oscillation in periodically poled $LiNbO_3$ with volume Bragg grating outcoupler
M. Henriksson, L. Sjöqvist, V. Pasiskevicius, F. Laurell
Applied Physics B: Lasers and Optics, **86**, 497-501 (2007)

This paper describes the first high repetition rate (10 kHz) OPO using a volume Bragg grating, and the first VBG OPO operating in the infrared. The OPO had 36 % conversion efficiency and 47 % slope efficiency and generated 1.56 W in the signal and idler at 2008 and 2264 nm, respectively.
Contribution by the author: The candidate performed the experiments. The candidate later wrote the paper with assistance from L. Sjöqvist, V. Pasiskevicius and F. Laurell.

Paper II
$ZnGeP_2$ Parametric Oscillator Pumped by a Linewidth Narrowed Parametric 2 μm Source
M. Henriksson, M. Tiihonen, V. Pasiskevicius and F. Laurell
Optics Letters, **31**, 1878-1880, (2006)

This paper is the first description of pumping of a ZGP OPO with the output of an OPO with a volume Bragg grating output coupler. A PPKTP OPO pumped by a 20 Hz PRF Nd:YAG laser produced a narrow bandwidth signal at 2008 nm through the use of a volume Bragg grating output coupler. The signal was used to pump a ZGP OPO generating broadband radiation in the 3-5 μm region. The ZGP OPO had a slope efficiency of 41 %, and the conversion efficiency of the whole tandem OPO setup was 4 % generating 170 μJ of output energy.
Contribution by the author: The candidate performed the experiments together with M. Tiihonen. The candidate wrote the paper with assistance from M. Tiihonen, V. Pasiskevicius and F. Laurell.

Paper III
Mid-infrared ZGP OPO pumped by near-degenerate narrowband type-I PPKTP parametric oscillator
M. Henriksson, M. Tiihonen, V. Pasiskevicius and F.Laurell
Applied Physics B Lasers and Optics, **88**, 37-41 (2007)

In this work we show a PPKTP OPO operating very close to degeneracy. The signal and idler peaks are 0.6 nm apart, and the full energy is contained in a 2 nm region. We also show efficient pumping of a ZGP OPO by the signal and the idler from the PPKTP OPO with a maximum slope efficiency of 43 %. The total slope efficiency from 1 μm to the 3.5-5 μm region was 10 % and the conversion efficiency was 7 %. Tuning from degeneracy to a signal wavelength below 3 μm with a corresponding idler wavelength at 8 μm was demonstrated.
Contribution by the author: The candidate performed the experiments. The candidate wrote the paper with assistance from M. Tiihonen, V. Pasiskevicius and F.Laurell.

Paper IV
Spectrum of Multi-Longitudinal Mode Pumped Near-Degenerate OPOs with Volume Bragg Grating Output Couplers
M. Henriksson, L. Sjöqvist, V. Pasiskevicius and F.Laurell
Optics Express **17**, 17582-17589 (2009)

This paper presents the first spectral characterisation of OPOs with VBG output couplers that resolve the longitudinal modes. The signal and idler at 2122 and 2135 nm were measured to 10 and 20 GHz FWHM bandwidth, respectively. With a 10 mm PPKTP crystal the signal spectrum is dominated by three longitudinal modes. Simulations of the effect of pump spectrum variation on the conversion efficiency of a ZGP OPO were also presented.
Contribution by the author: The candidate performed the experiments. The paper was written by the candidate and V. Pasiskevicius with assistance from L. Sjöqvist and F.Laurell.

Paper V
Cavity length resonances in a nanosecond singly resonant optical parametric oscillator
M. Henriksson, L. Sjöqvist, V. Pasiskevicius and F.Laurell
Submitted to Optics Express

Cavity length resonances with increased output energy when the cavity lengths of laser and OPO match are a known phenomenon from DROs. This paper presents the first experimental demonstration of cavity length resonances in a nanosecond SRO. The VBG was used to ensure that there was no feedback at the idler wavelength, something that would not be possible with a dielectric mirror. The cause of the cavity length resonances in the SRO are cross-correlation of the periodic intensity spike patterns in signal and idler. The cross-correlation is destroyed by length mismatches larger than the inverse bandwidth and by operation high above threshold.
Contribution by the author: The candidate performed the experiments. The paper was written by the candidate and V. Pasiskevicius with assistance from L. Sjöqvist and F.Laurell.

7. Conclusions

In this thesis I have presented a new method for generating mid-infrared radiation through a tandem OPO setup pumped by a 1.06 μm Nd-laser. The new invention is to use a volume Bragg grating as a cavity mirror in a near degenerate quasi phase-matched OPO to generate the narrow bandwidth 2.1 μm radiation that is needed to pump a mid-IR ZGP OPO. The main advantages of this method compared to traditional bulk KTP type II OPOs are that the QPM crystals (PPLN or PPKTP) provide higher nonlinearity and avoid walk-off and that the signal and idler have the same polarisation and can both be used to pump the ZGP OPO simultaneously. The use of a VBG for spectral narrowing is more efficient than other methods, such as etalons and surface relief gratings, since no additional components are needed in the cavity and the cavity length can be kept short.

With the help of the narrow bandwidth reflection peak of the VBG an OPO where the signal and idler at 2122 and 2135 nm were limited to 10 GHz and 20 GHz FWHM bandwidth, respectively, has been demonstrated. This should be compared to a PPKTP OPO using dielectric mirrors that may have over 200 nm bandwidth around degeneracy. The total output energy generated in the PPKTP OPO (signal and idler together) has been used to pump a ZGP OPO that produced mid-IR radiation. Tuning of the signal from a ZGP OPO from 2.9 μm to degeneracy at 4.3 μm has been shown, with a corresponding idler wavelength up to 8 μm. The spectrum could especially be tuned to be a good fit of the mid-IR atmospheric transmission windows in the 3.5 to 5 μm wavelength range and thus well suited to the DIRCM application that motivated this work. The highest conversion efficiency that has been reached from 1.06 μm to the mid-IR was 12 %. This setup used a PPKTP OPO with 30 % conversion efficiency and 13 nm separation of signal and idler (2122 and 2135 nm). The setup was running at 20 kHz PRF and generated 3.2 W output power in the mid-IR.

By using a VBG output coupler to ensure single resonance of the OPO the existence of cavity length resonances in SROs was proven. This was a known phenomenon from doubly resonant OPOs, but for SROs only a simulation existed. The increase in the OPO efficiency when the OPO cavity length is equal to or a fraction of the laser cavity length is in the SRO case caused by the periodicity of the spiking pattern of the pump laser. If the roundtrip times of OPO and laser match there will be cross-correlation of the spiking in laser and OPO. The single pass gain will then be higher and the threshold reduced compared to if the lengths do not match.

7.1. Outlook

Even though relatively good conversion efficiency from 1.06 μm to the mid-IR of 12 % has been demonstrated in this thesis, this is not believed to be the maximum possible. For a tandem setup only two different VBGs have been tested in a PPKTP OPO, and those two tests used different pump lasers so they could not be properly compared. In addition the only difference between the VBGs was the resonance wavelength. Optimization concerning peak diffraction efficiency and VBG bandwidth has not been studied at all. The effects of the resonance wavelength and hence the separation of signal and idler are certainly also important. The ZGP OPO should, as the simulation results show, be more efficient the closer the two pump components are. On the other hand it is possible that the parasitic FWM will reduce the efficiency of the first OPO closer to degeneracy, and in addition reduce the pumping efficiency of the second OPO. The variation of the FWM with the distance from degeneracy and

the actual effect of the FWM on the conversion efficiency of the tandem setup have so far not been investigated. In total it is possible that there is an optimum non-zero separation of signal and idler in the first OPO. There may also be possibilities to increase the efficiency by optimizing the pump focusing and by using a curved incoupling mirror.

In cavities where the mode separation, through short cavity lengths and/or narrow bandwidth VBGs, is on the same order of magnitude as the VBG bandwidth fine adjustment of the mode frequencies relative to the Bragg resonance peak will be important for the effective reflectivity. By adjusting the mode comb so that one mode is at the peak, or so that the peak is between two modes clearly different mode spectra should be obtainable. The effects of this fine tuning on efficiency and bandwidth has so far not been investigated.

Further interesting experiments to study could be the use of a single longitudinal mode pump laser, possibly together with a VBG with narrower reflection bandwidth to limit the operation to a single longitudinal mode. The behaviour of this type of OPO exactly at degeneracy for true wavelength doubling should be possible to investigate by temperature tuning of a VBG resonant close to degeneracy.

So far most of the experiments have been performed using PPKTP and ZGP. The single experiment using a PPLN crystal was performed far away from degeneracy and was never used to pump a ZGP OPO. The narrower gain bandwidths of other QPM materials could reduce the parasitic FWM and possibly increase the efficiency. It would also be very interesting to try pumping of an OP-GaAs OPO. No significant differences in performance to the so far published experiments are expected from this, but the narrower acceptance bandwidth of OP-GaAs compared to ZGP may further prove the value of the demonstrated bandwidth narrowing.

References

1. C. Peña, "Flying the unfriendly skies, Defending against the threat of shoulder fired missiles," Policy analysis No. 541, Cato Institute (2005).
2. The Air Force Research Laboratory, Space Vehicles Directorate, MODTRAN 4 Software, http://www.kirtland.af.mil/library/factsheets/factsheet.asp?id=7915.
3. D. Titterton, "A consideration of the requirements for laser devices used in countermeasure applications," Proc. SPIE **6451**, 64511Q (2007).
4. A. Godard, "Infrared (2-12 µm) solid-state laser sources: a review, Comptes Rendus Physique **8**, 1100-1128 (2007).
5. J. C. Shin, M. D'Souza, Z. Liu, J. Kirch, L. J. Mawst, D. Botez, I. Vurgaftman, and J. R. Meyer, "Highly temperature insensitive, deep-well 4.8 µm emitting quantum cascade semiconductor lasers," Appl. Phys. Lett. **94**, 201103 (2009).
6. J. A. Giordmaine and Robert C. Miller, "Tunable Coherent Parametric Oscillation in $LiNbO_3$ at Optical Frequencies," Phys. Rev. Lett. **14**, 973–976 (1965).
7. P. A. Budni, L. A. Pomeranz, M. L. Lemons, C. A. Miller, J. R. Mosto, and E. P. Chicklis, "Efficient mid-infrared laser using 1.9- µm-pumped Ho:YAG and $ZnGeP_2$ optical parametric oscillators," J. Opt. Soc. Am. B **17**, 723-728 (2000).
8. E. Lippert, S. Nicolas, G. Arisholm, K. Stenersen, and G. Rustad, "Midinfrared laser source with high power and beam quality," Appl. Opt. **45**, 3839 (2006).
9. S. Haidar, K. Miyamoto, and H. Ito, "Generation of tunable mid-IR (5.5–9.3 µm) from a 2-µm pumped $ZnGeP_2$ optical parametric oscillator," Opt. Comm. **241**, 173-178 (2004).
10. E. Cheung, S. Palese, H. Injeyan, C. Hoefer, R. Hilyard, H. Komine, J. Gish and W. Bosenberg, "High power optical parametric oscillator source," in Proceedings of IEEE Aerospace Conference (Institute of Electrical and Electronics Engineers, New York, 2000), 55-59, vol. 3.
11. G. Arisholm, E. Lippert, G. Rustad, and K. Stenersen, "Efficient conversion from 1 to 2 µm by a KTP-based ring optical parametric oscillator", Opt. Lett. **27**, 1336-1338 (2002).
12. J. A. C. Terry, K. J. McEwan, and M. J. P. Payne, "A Tandem OPO route to the mid-IR," in *Advanced Solid State Lasers*, W. Bosenberg and M. Fejer, eds., Vol. 19 of OSA Trends in Optics and Photonics Series (Optical Society of America, 1998), paper FC4.
13. P. B. Phua, B.S. Tan, R. F. Wu, K. S. Lai L. Chia and E. Lau, "High-average-power mid-infrared $ZnGeP_2$ optical parametric oscillator with a wavelength-dependent polarization rotator," Opt. Lett. **31**, 489-451 (2006).
14. K. Miyamoto, K. Suizu, H. Ito, "A wavelength-agile mid-IR (5-10µm) light source pumped by a Galvano-controlled KTP-OPO," Lasers and Electro-Optics Society, 2005. LEOS 2005. The 18th Annual Meeting of the IEEE, p 1663-1664, paper TuV2 (2005).
15. B. Jacobsson, M. Tiihonen, V. Pasiskevicius, and F. Laurell, "Narrowband bulk Bragg grating optical parametric oscillator," Opt. Lett. **30**, 2281-2283 (2005).
16. M. Mackanos, "The effect of pulse structure on soft tissue laser ablation at mid-infrared wavelengths," PhD-thesis, URN etd-11292004-165251., Vanderbilt University, USA, (2004).
17. MIRSURG (Mid-Infrared Solid-State Laser Systems for Minimally Invasive Surgery), EU research program, Grant agreement No. 224042.

18. G. Arisholm, E. Lippert, G. Rustad, and K. Stenersen, "Effect of resonator length on a doubly resonant optical parametric oscillator pumped by a multilongitudinal-mode beam," Opt. Lett. **25**, 1654-1656 (2000).
19. P. N. Butcher and D. Cotter, The elements of nonlinear optics, Eds. P. L. Knight and W. J. Firth, Cambridge Studies in modern optics:9, Cambridge university press, UK (1990).
20. R. L. Sutherland, Handbook of nonlinear optics, 2nd ed., Marcel Dekker Inc., New York (2003).
21. D. J. Armstrong, W. J. Alford, T. D. Raymond, A. V. Smith, and M. S. Bowers, "Parametric amplification and oscillation with walkoff-compensating crystals," J. Opt. Soc. Am. B **14**, 460- (1997).
22. J. A. Armstrong, N. Bloembergen, J. Ducuing, and P. S. Pershan, "Interactions between Light Waves in a Nonlinear Dielectric," Phys., Rev. **127**, 1918-1939 (1962).
23. M. Yamada, N.Nada, M. Saitoh and K. Watanabe, "First-order quasi-phase matched $LiNbO_3$ waveguide periodically poled by applying an external field for efficient blue second-harmonic generation," Appl. Phys. Letts. **62**, 435-436 (1993).
24. J. Webjorn, V. Pruneri, P.S.J. Russell, J.R.M. Barr and D.C. Hanna, "Quasi-phase-matched blue light generation in bulk lithium niobate, electrically poled via periodic liquid electrodes," Electron. Lett. **30**, 894-895 (1994).
25. SNLO nonlinear optics code available from A. V. Smith, AS-Photonics, Albuquerque, NM.
26. R. W. Boyd, Nonlinear Optics, Academic, San Diego, (1992), Chap. 2.
27. G. Arisholm, G. Rustad, and K. Stenersen, "Importance of pump-beam group velocity for backconversion in optical parametric oscillators," J. Opt. Soc. Am. B **18**, 1882-1890 (2001).
28. T. Debuisschert, J. Raffy, J-M. Dupont, and J-P. Pocholle, "Optical parametric oscillators: Basics and applications Nanosecond optical parametric oscillators," C. R. Acad. Sci. Paris, t. 1, Série IV, 561-583 (2000).
29. M. H. Dunn and M. Ebrahimzadeh, "Parametric generation of tunable light from continuous-wave to femtosecond pulses," Science **286**, 1513-1517 (1999).
30. S. E. Harris, "Tunable Optical Parametric Oscillators," Proc. IEEE **57**, 2096 (1969).
31. G. Arisholm and K. Stenersen, "Optical parametric oscillator with non-ideal mirrors and single- and multi-mode pump beams," Opt. Express **4**, 183-192 (1999).
32. S. Brosnan and R. Byer, "Optical Parametric Oscillator Threshold and Linewidth Studies," IEEE J. Quantum Electron. **15**, 415- (1979).
33. K. L. Vodopyanov and P. G. Schunemann, "Broadly tunable noncritically phase-matched $ZnGeP_2$ optical parametric oscillator with a 2-μJ pump threshold," Opt. Lett. **28**, 441-443 (2003).
34. Bjorkholm, J., "Some effects of spatially nonuniform pumping in pulsed optical parametric oscillators," IEEE Journal of Quantum Electronics **7**, 109–118 (1971).
35. G. D. Boyd and D. A. Kleinman, "Parametric interaction of focused Gaussian light beams," J. Appl. Phys. **39**, 3597- (1968).
36. L. E. Myers, G. D. Miller, R. C. Eckardt, M. M. Fejer, R. L. Byer, "Quasi-phase-matched 1.064 μm pumped optical parametric oscillator in bulk periodically poled $LiNbO_3$," Opt. Lett. **20**, 52-54 (1995).

37. I. Shoji, T. Kondo, A. Kitamoto, M. Shirane, and R. Ito, "Absolute scale of second-order nonlinear-optical coefficients," J. Opt. Soc. Am. B **14**, 2268-(1997).
38. H. Ishizuki and T. Taira, "High-energy quasi-phase-matched optical parametric oscillation in a periodically poled MgO:$LiNbO_3$ device with a 5 mm×5 mm aperture," Opt. Lett. **30**, 2918-2920 (2005).
39. N. E. Yu, S. Kurimura, Y. Nomura, M. Nakamura, K. Kitamura, Y. Takada, J. Sakuma, and T. Sumiyoshi, "Efficient optical parametric oscillation based on periodically poled 1.0 mol % MgO-doped stoichiometric $LiTaO_3$," Appl. Phys. Lett. **85**, 5134-5136 (2004).
40. J. Hellström, V. Pasiskevicius, H. Karlsson, and F. Laurell, "High-power optical parametric oscillation in large-aperture periodically poled $KTiOPO_4$," Opt. Lett. **25**, 174-176 (2000).
41. M. V. Pack, D. J. Armstrong, and A. V. Smith, "Measurement of the chi^(2) Tensors of $KTiOPO_4$, $KTiOAsO_4$, $RbTiOPO_4$, and $RbTiOAsO_4$ Crystals," Appl. Opt. **43**, 3319-3323 (2004).
42. G. Hansson, H. Karlsson, S. Wang, and F. Laurell, "Transmission Measurements in KTP and Isomorphic Compounds," Appl. Opt. **39**, 5058-5069 (2000).
43. G. Anstett, F. Ruebel, and J. L'huillier, "Generation of Powerful Tunable Mid-Infrared Picosecond Laser Radiation Using Frequency Conversion in Periodically Poled Lithium Niobate," in Advanced Solid-State Photonics, OSA Technical Digest Series (CD) (Optical Society of America, 2010), paper AWD3.
44. A. Tyazhev, G. Marchev, V. Vedenyapin, D. Kolker, A. Yelisseyev, S. Lobanov, L. Isaenko, J.-J. Zondy, and V. Petrov, "$LiInSe_2$ nanosecond optical parametric oscillator tunable from 4.7 to 8.7 μm," Proc. SPIE **7582**, 75820E (2010).
45. P. G. Schunemann, K. T. Zawilski, T. M. Pollak, D. E. Zelmon, N. C. Fernelius, and F. K. Hopkins, "New Nonlinear Optical Crystal for Mid-IR OPOs: $CdSiP_2$," in Advanced Solid-State Photonics, OSA Technical Digest Series (CD) (Optical Society of America, 2008), paper MG6.
46. V. Petrov, P. G. Schunemann, K. T. Zawilski, and T. M. Pollak, "Noncritical singly resonant optical parametric oscillator operation near 6.2 μm based on a $CdSiP_2$ crystal pumped at 1064 nm," Opt. Lett. **34**, 2399-2401 (2009)
47. Y. X. Fan, R. C. Eckardt, R. L. Byer, R. K. Route and R. S. Feigelson, "$AgGaS_2$ infrared parametric oscillator," Appl. Phys. Lett. **45**, 313-315 (1984).
48. K. L. Vodopyanov, J. P. Maffetone, I. Zwieback, and W. Ruderman, "$AgGaS_2$ optical parametric oscillator continuously tunable from 3.9 to 11.3 μm," Appl. Phys. Lett. **75**, 1204-1206 (1999).
49. R. C. Eckardt, Y. X. Fan, R. L. Byer, C. L. Marquardt, M. E. Storm, and L. Esterowitz, "Broadly tunable infrared parametric oscillator using $AgGaSe_2$," Appl. Phys. Lett. **49**, 608-610 (1986).
50. S. Chandra, T. H. Allik, G. Catella, R. Utano and J. A. Hutchinson, "Continuously tunable, 6–14 μm silver-gallium selenide optical parametric oscillator pumped at 1.57 μm," Appl. Phys. Lett. **71**, 584-586 (1997).
51. G.D. Boyd, E. Buehler and F.G. Storz, "Linear and nonlinear optical properties of $ZnGeP_2$ and CdSe," Appl. Phys. Lett. **18**, 301-304 (1971).
52. H. M. Hobgood, T. Henningsen, R. N. Thomas, R. H. Hopkins, M. C. Ohmer, W. C. Mitchel, D. W. Fischer, S. M. Hegde, and E K. Hopkins, "$ZnGeP_2$ grown

by the liquid encapsulated Czochralski method," J. Appl. Phys. **73**, 4030-4037 (1992).
53. Y. Isyanova, G. A. Rines, D. Welford, and P. F. Moulton, "Tandem OPO Source Generating 1.5-10-μm Wavelengths," in *Advanced Solid State Lasers*, S. Payne and C. Pollack, eds., Vol. 1 of OSA Trends in Optics and Photonics Series (Optical Society of America, 1996), paper OP10.
54. A. Zakel, S. D. Setzler, P. G. Schunemann, T. M. Pollak, M. Burky, S. Guha, "Optical parametric oscillator based on cadmium germanium arsenide," in Conference on Lasers and Electro-Optics (CLEO 2002), Tech. Digest (Optical Society of America, 2002), p. 172.
55. P. D. Mason, E. J. McBrearty, P. J. Webber, B. J. Perrett, M. R. Wedd, D. A. Orchard, "Improved multi-layer glass-bonded QPM GaAs crystals for non-linear wavelength conversion into the mid-infrared," Proc. SPIE **5990**, 599005 (2005).
56. C. B. Ebert, L. A. Eyres, M. M. Fejer, and J. S. Harris, "MBE growth of antiphase GaAs films using GaAs/Ge/GaAs heteroepitaxy," J. Cryst. Growth **201**, 187-193 (1999).
57. S. Koh, T. Kondo, Y. Shiraki, and R. Ito, "GaAs/Ge/GaAs sublattice reversal epitaxy and its application to nonlinear optical devices," J. Cryst. Growth **227**, 183 (2001).
58. L. A. Eyres, P. J. Tourreau, T. J. Pinguet, C. B. Ebert, J. S. Harris, M. M. Fejer, L. Becouarn, B. Gerard, and E. Lallier, "All-epitaxial fabrication of thick, orientation-patterned GaAs films for nonlinear optical frequency conversion," Appl. Phys. Lett. **79**, 904 (2001).
59. C. Kieleck, M. Eichhorn, A. Hirth, D. Faye, and E. Lallier, "High-efficiency 20–50 kHz mid-infrared orientation-patterned GaAs optical parametric oscillator pumped by a 2 μm holmium laser," Opt. Lett. **34,** 262-264 (2009).
60. I. Tomita, H. Suzuki, H. Ito, H. Takenouchi, K. Ajito, R. Rungsawang, and Y. Ueno, "Terahertz-wave generation from quasi-phase-matched GaP for 1.55 μm pumping," Appl. Phys. Lett. **88**, 071118 (2006).
61. M. T. Kelemen, J. Gilly, M. Haag, J. Biesenbach, M. Rattunde, J. Wagner, "Diode laser arrays for the 1.8 to 2.2 μm range", Proc. SPIE **7230**, 72301K (2009).
62. A. Zakel, G. J. Wagner, W. J. Alford, and T. J. Carrig, "High-Power, Rapidly-Tunable $ZnGeP_2$ Intracavity Optical Parametric Oscillator," in *Conference on Lasers and Electro-Optics/Quantum Electronics and Laser Science and Photonic Applications Systems Technologies*, Technical Digest (CD) (Optical Society of America, 2005), paper CThY5.
63. D. Creeden, P. A. Ketteridge, P. A. Budni, S. D. Setzler, Y. E. Young, J. C. McCarthy, K. Zawilski, P. G. Schunemann, T. M. Pollak, E. P. Chicklis, and M. Jiang, "Mid-infrared $ZnGeP_2$ parametric oscillator directly pumped by a pulsed 2 μm Tm-doped fiber laser," Opt. Lett. **33**, 315-317 (2008).
64. C. Kieleck, M. Eichhorn, D. Faye, E. Lallier, and S. D. Jackson, "Polarization effects and fiber-laser-pumping of a 2-μm-pumped OP-GaAs OPO," Proc. SPIE **7582**, 758212 (2010).
65. D. E. Smith, M. S. Bowers, P. G. Schunemann, "Multiwavelength mid-infrared zinc germanium phosphide and PPLN optical parametric oscillator," Proc. SPIE **4972**, 78 (2003).
66. G. Kalmani, A. Arie, P. Blau, S. Pearl, and A.V. Smith, "Polarization-mixing optical parametric oscillator," Opt. Lett. **30**, 2146-2148 (2005).

67. B. Perrett, J.Terry, P. Mason, D. Orchard, "Spectral line narrowing in PPLN OPO devices for 1 μm wavelength doubling," Proc. SPIE **5620**, 275-283 (2004).
68. J. Saikawa, M. Fujii, H. Ishizuki, and T. Taira, "52 mJ narrow-bandwidth degenerated optical parametric system with a large-aperture periodically poled MgO:$LiNbO_3$ device," Opt. Lett. **31**, 3149-3151 (2006).
69. K. T. Zawilski, S. D. Setzler, P. G. Schunemann, and T. M. Pollak, "Increasing the laser-induced damage threshold of single-crystal $ZnGeP_2$," J. Opt. Soc. Am. B **23**, 2310-2316 (2006)
70. N. C. Giles, L. Bai, M. M. Chirila, N. Y. Garces, K. T. Stevens, P. G. Schunemann, S. D. Setzler and, T. M. Pollak, "Infrared absorption bands associated with native defects in $ZnGeP_2$," J. of Appl. Phys. **93**, 8975-8981 (2003).
71. G. Arisholm, "General numerical methods for simulating second-order nonlinear interactions in birefringent media," J. Opt. Soc. Am. B **14**, 2543-2549 (1997).
72. G. Arisholm, "Advanced numerical simulation models for second-order nonlinear interactions," Proc. SPIE **3685**, 86-97 (1999).
73. B. Jacobsson, "Spectral control of lasers and optical parametric oscillators with volume Bragg gratings," PhD-thesis, Trita-FYS 2008:13, KTH, Stockholm, Sweden (2008).
74. O. Efimov, L. Glebov, L. Glebova, K. Richardson, and V. Smirnov, "High-efficiency Bragg gratings in photothermorefractive glass," Appl. Opt. **38**, 619–627 (1999).
75. H. Kogelnik, "Coupled wave theory for thick hologram gratings," Bell Syst. Tech. J. **48**, 2909-2947 (1969).
76. P. Blau, S. Pearl, S. Fastig and R. Lavi, "Single-Mode Operation of a Mid-Infrared Optical Parametric Oscillator Using Volume-Bragg-Grating Cavity Mirrors," IEEE J. Quant. Elec. **44**, 867-871 (2008).
77. A. J. Merriam, V. Smirnov, and L. Glebov, "Spectral narrowing and tunability of a high-power diffraction-limited ns-pulsed OPO/OPA system using transversely-chirped and temperature-tuned volume Bragg gratings," Proc. SPIE **7193**, 71930R (2009).
78. J. Lumeau, L. B. Glebov, and V. Smirnov, "Tunable narrowband filter based on a combination of Fabry-Perot etalon and volume Bragg grating," Opt. Lett. **31**, 2417-2419 (2006).
79. A. Sevian, O. Andrusyak, I. Ciapurin, V. Smirnov, G. Venus, and L. Glebov, "Efficient power scaling of laser radiation by spectral beam combining," Opt. Lett. **33**, 384-386 (2008).
80. K.-H. Liao, M.-Y. Cheng, E. Flecher, V. I. Smirnov, L. B. Glebov, and A. Galvanauskas, "Large-aperture chirped volume Bragg grating based fiber CPA system," Opt. Express **15**, 4876-4882 (2007).
81. L. Glebov, "High brightness laser design based on volume Bragg gratings," Proc. SPIE **6216**, 621601 (2006).
82. B. Volodin, S. Dolgy, E. Melnik, E. Downs, J. Shaw, and V. Ban, "Wavelength stabilization and spectrum narrowing of high-power multimode laser diodes and arrays by use of volume Bragg gratings," Opt. Lett. **29**, 1891–1893 (2004).
83. B. Jacobsson, V. Pasiskevicius, and F. Laurell, "Single-longitudinal-mode Nd-laser with a Bragg-grating Fabry-Perot cavity," Opt. Express **14**, 9284-9292 (2006).

84. B. Jacobsson, V. Pasiskevicius, and F. Laurell, "Tunable single-longitudinal-mode ErYb:glass laser locked by a bulk glass Bragg grating," Opt. Lett. **31**, 1663-1665 (2006).
85. A. Dergachev, P. F. Moulton, V. Smirnov, and L. Glebov, "High power CW Tm:YLF laser with a holographic output coupler," in Conference on Lasers and Electro-Optics/International Quantum Electronics Conference and Photonic Applications Systems Technologies, Technical Digest (CD) (Optical Society of America, 2004), paper CThZ3.
86. P. Jelger and F. Laurell, "Efficient narrow-linewidth volume-Bragg grating-locked Nd:fiber laser," Opt. Express **15**, 11336-11340 (2007).
87. B. Jacobsson, C. Canalias, V. Pasiskevicius, and F. Laurell, "Narrowband and tunable ring optical parametric oscillator with a volume Bragg grating," Opt. Lett. **32**, 3278-3280 (2007).
88. B. Jacobsson, V. Pasiskevicius, F. Laurell, E. Rotari, V. Smirnov, and L. Glebov, "Tunable narrowband optical parametric oscillator using a transversely chirped Bragg grating," Opt. Lett. **34**, 449-451 (2009).
89. J. Saikawa, M. Fujii, H. Ishizuki, and T. Taira, "High-energy, narrow-bandwidth periodically poled Mg-doped $LiNbO_3$ optical parametric oscillator with a volume Bragg grating," Opt. Lett. **32**, 2996-2998 (2007).
90. A. J. Merriam, J. J. Jacob, D. S. Bethune, and J. A. Hoffnagle, "Efficient Nonlinear Frequency Conversion to 193-nm Using Cooled BBO," in Advanced Solid-State Photonics, OSA Technical Digest Series (CD) (Optical Society of America, 2007), paper MB11.
91. J. Jacob, D. Armstrong, and A. Smith, "Far-UV solid state lasers for semiconductor processing," Proc. SPIE **7582**, 75820U (2010).
92. J. Saikawa, M. Miyazaki, M. Fujii, H. Ishizuki, and T. Taira, "High-energy, broadly tunable, narrow-bandwidth mid-infrared optical parametric system pumped by quasi-phase-matched devices," Opt. Lett. **33**, 1699-1701 (2008).
93. M. Vainio, M. Siltanen, T. Hieta, and L. Halonen, "Continuous-wave optical parametric oscillator based on a Bragg grating," Opt. Lett., doc. ID 124503 (posted 29 March 2010, in press).
94. K. Ait-Ameur, F. Sanchez, "Transverse effects as source of error in coherence length measurements," Opt. Comm. **233**, 39-43 (2004).
95. H. Huang, J. He, X. Fan, Y. Zhong, H. Chai, and Y. Wang, "The acousto-optic Q-switched mode-locking Nd:YVO4 laser," Optics & Laser Technology **40**, 828-831 (2008).
96. S. Harris, "Threshold of multimode parametric oscillators," IEEE J. Quant. Elec. **2**, 701-701 (1966).
97. R. L. Byer, M. K. Oshman, J. F. Young, and S. E. Harris, "Visible CW parametric oscillator," Appl. Phys. Lett. **13**, 109-111 (1968).
98. G. Rustad, E. Lippert, K. Stenersen, and G. Arisholm, "Enhanced power from a doubly resonant optical parametric oscillator by choice of resonator length," in Advanced Solid-State Lasers, C. Marshall, ed., Vol. 50 of OSA Trends in Optics and Photonics (Optical Society of America, 2001), paper WD5.
99. K. Burneika, M. Ignatavicius, V. Kabclka, A. Piskarskas, and A. Stabinis, "Parametric light amplification and oscillation in KDP with mode-locked pump," IEEE J. Quantum Electron. **8**, 574 (1972).
100. E. C. Cheung and J. M. Liu, "Theory of a synchronously pumped optical parametric oscillator in steady-state operation," J. Opt. Soc. Am. B **7**, 1385-1401 (1990).

101. D. H. Titterton, “A review of the development of optical countermeasures,” Proc. SPIE **5615**, 1 (2004),
102. The infrared & electro-optical systems handbook, Volume 7 Countermeasure systems, D. H. Pollock, Ed., Chapter 3, SPIE Optical engineering press, Bellingham, USA (1993).
103. The infrared & electro-optical systems handbook, Volume 2 Atmospheric propagation of radiation, F. G. Smith, Ed., p. 253-254, SPIE Optical engineering press, Bellingham, USA (1993).
104. A. N. Kolmogorov, “The local structure of turbulence in incompressible viscous fluid for very large Reynolds numbers,” C. R. Acad. Sci. URSS **36**, 301 (1941).
105. L. Sjöqvist, “Laser beam propagation in jet engine plume environments: a review,” Proc. SPIE **7115**, 71150C (2008).
106. L. C. Andrews and R. L. Phillips, Laser beam propagation through random media, SPIE Press, Bellingham, USA (2005).